ATTACHMENT 9

Westinghouse WCAP-17330-NP, Revision 1

H*: Resolution of NRC Technical Issue Regarding Tubesheet Bore Eccentricity (Model F/Model D5)

(Non-Proprietary)

Westinghouse Non-Proprietary Class 3

WCAP-17330-NP
Revision 1

June 2011

H*: Resolution of NRC Technical Issue Regarding Tubesheet Bore Eccentricity (Model F/Model D5)

WCAP-17330-NP
Revision 1

H*: Resolution of NRC Technical Issue Regarding Tubesheet Bore Eccentricity (Model F/Model D5)

W. J. Bedont*
SG Design and Analysis

C. D. Cassino*
SG Design and Analysis

A. O. Roslund*
SG Design and Analysis

G. W. Whiteman*
SG Design and Analysis

June 2011

Reviewer: H. O. Lagally*
SG Management Programs

Approved: D. A. Testa*, Manager
SG Management Programs

*Electronically approved records are authenticated in the electronic document management system.

Westinghouse Electric Company LLC
1000 Westinghouse Drive
Cranberry Township, PA 16066, USA

REVISION RECORD

Revision No.		Date of Issue
0	Original Issue	11/10
1	Section 1; editorial modifications, added Section 1.3 to summarize independent review Section 2; added introductory statement Section 2.1; editorial changes Section 2.3.1; modified third paragraph Section 2.5; expanded meshing discussion, added convergence criteria and added discussion on artificial stiffness Section 3.2.2; expanded discussion on SLB analysis; editorial changes in discussion of divider plate Section 3.2.4; expanded discussion on divider plate modeling Section 3.2.5; editorial changes only Section 3.2.8; editorial changes only Section 3.3.3, 3.3.4, 3.3.6; editorial changes only Section 3.3.9; now includes prior Section 3.3.11 Section 3.3.10; now includes prior Section 3.3.12 Tables 3-8 through 3-19; data added for additional elevations Figures 3-19 through 3-29; data added for additional elevations Section 3.3.11; replaces prior Section 3.3.13, added discussion on calculation process and effect of Poisson contraction Section 3.3.12; new section: "Axial Location of Departure from Zero Contact Pressure" Section 3.3.13; new section: "Circumferential Contact Pressure" Added Table 3-22 Added Figure 3-30 through 3-35; Circumferential Contact pressure for Model D5 and Model F Section 3.4; re-written in its entirety Section 3.5; modified to reflect minor process change to account for added axial elevations and to eliminate apparent contradictions in original Tables 3-40 (3-39 in this Rev.) and 3-46 (3-49 in this Rev.) Section 3.6; new section for crevice pressure adjustment length; replaces discussion in Section 3.4 in Rev. 0 Section 3.7; new summary section; replaces discussion in Section 3.4 in Rev. 0	06/11

TABLE OF CONTENTS

TABLE OF CONTENTS (cont.)

LIST OF TABLES

LIST OF TABLES (cont.)

LIST OF TABLES (cont.)

LIST OF FIGURES

LIST OF FIGURES (cont.)

LIST OF FIGURES (cont.)

1 INTRODUCTION

The purpose of H* is to replace the tube-end weld with the hydraulic expansion joint as the primary pressure boundary in the SG. There are two principal requirements for H*:

1. Assure that the tube(s) do not pull out of the tubesheet under the most limiting loads during normal operating or accident conditions.

2. Assure that the primary coolant leakage through the tube-to-tubesheet crevice is no greater than the leakage assumed in the final safety analysis report (FSAR) for the most limiting accident.

After withdrawal of the first permanent license amendment requests in 2008, the industry addressed the questions posed by the U.S. Nuclear Regulatory Commission (NRC) about the technical analysis, and in September 2009, the NRC issued its first of several approvals of H* that recognizes the hydraulic expansion joint as the primary pressure boundary (Reference 1-1, typical). The approval in each case was limited to the operating period until the plant's next scheduled inspection because, as stated by the NRC, one technical issue remained to be resolved. The technical issue revolves around the relationship between tubesheet bore eccentricity and the tube-to-tubesheet contact pressure. This issue was identified in Reference 1-2, which provided 14 questions related to this issue. (Although Reference 1-2 is not a formal request for additional information (RAI), it will be referred to in this report as an RAI.) The purpose of this report, in conjunction with References 1-6 and 1-7, is to provide final resolution of the remaining questions in support of the permanent application of the H* criterion. The remaining eccentricity issue impacts both the structural and leakage analysis aspects of the H* analysis.

In this report, reference to the "current licensing basis" means the basis on which the temporary licenses were provided to the Model F and Model D5 plants. Principally, the technical basis for the current licensing basis is contained in WCAP-17071-P, Rev. 2 (Reference 1-3) and WCAP-17072-P (Reference 1-4), but also includes other documents included in the respective License Amendment Requests (LARs) from the respective Model F and Model D5 plants.

1.1 ORIGINAL NRC RAI RESOLUTION ACTION PLAN DISCUSSION

Westinghouse initially interpreted the thrust of the questions as follows:

The H* structural justification includes an analysis that determines the contact pressure between the tubes and the tubesheet. The reference model for this calculation, the "Scale Factor Model" (SF) is a previously documented model (Reference 1-5) developed to determine the contact pressure for various values of dilation and eccentricity of the tubesheet bore. The output of this model is a multiplier to be applied to the calculated value of contact pressure due to tubesheet bore dilation, which is subtracted from the contact pressure generated due to tube-to-tubesheet differential thermal and pressure expansions. Because the transient conditions for one model (D5) of the affected steam generators required application of this model for conditions outside of the applicability of the reference model, a second model, the "Square-Cell Model" (C^2), a two-dimensional (2-D) finite element analysis (FEA), was utilized to directly determine the contact loads between the tubes and the tubesheet for these conditions.

Both models are based on conservative analysis and assumptions; however, Westinghouse believes that the C^2 model more accurately represents the physical structure. Originally, the principal purpose of the C^2 model was to demonstrate that adequate contact pressure exists around the circumference of the tube under significant tubesheet bore eccentricity conditions. The two models, SF and C^2, are entirely different approaches; thus it is not expected that the results from both models provide the same results. Westinghouse believed that, in aggregate, the NRC unresolved issue questions requested a comparison of the models and rationalization of the conservatism of the current licensing basis.

During a meeting in January 2010 with the NRC and the industry participants, Westinghouse proposed a plan to resolve all of the NRC questions through an approach believed to minimize the potential for additional questions. The NRC staff did not reject the recommended approach but stated that the 14 questions provided by Reference 1-2 must be clearly, if not directly, addressed. The target date established for a permanent H* license was the Spring 2011 outages. It was expected at the time that the contact pressures developed using the C^2 model would be of such a magnitude that the conservatism of the original licensing basis from both a structural and leakage integrity basis would be readily demonstrated.

1.2 REVISED NRC RAI RESOLUTION ACTION PLAN DISCUSSION

The Westinghouse action plan to respond to the 14 RAI questions, presented at the January 2010 meeting, was revised as discussed below.

1.2.1 Road Map to Final Response to 14 NRC RAI Except RAI #5 and RAI #12

It was determined by the NRC staff that the issues related to the SF model were resolved and that within the context of the SF model, eccentricity does not appear to be a significant variable affecting the tube-to-tubesheet contact pressure or calculated H* distances. This conclusion is based largely on the information provided in References 1-6 and 1-7 (LTR-SGMP-10-78 P-Attachment and LTR-SGMP-10-33 P-Attachment). From this information, the NRC staff concluded in Reference 1-8 that several of the NRC questions no longer require specific answers. Reference 1-7 provides a final response for each of the 14 remaining questions except RAI Questions #5 and #12, which address the C^2 model specifically. A more detailed description of the C^2 model, necessary to complete this remaining action, is provided by this report.

1.2.2 Need for Alternate Leakage Factor Approach

The Darcy formulation was used in References 1-3 and 1-4 to develop the ratio of leak rates between postulated accident induced conditions (SLB/FLB) and normal operating conditions (NOP). The driving heads (Δp) at both of these conditions are known, as are the temperatures and pressures to define the fluid viscosity (μ). In References 1-3 and 1-4, because the physical length of the leak path was the same under both normal operating and accident conditions, the length of the leak path was not a factor. The only remaining factor was the loss coefficient (K). Based on the analyses using the C^2 model, the length of the leak paths under normal operating conditions and accident conditions may differ; therefore, the SLB:NOP leak rate ratio is re-evaluated in Section 4 of this report.

The available data for hydraulically expanded tubes in tubesheet simulants (References 1-9 and 1-10), both at room temperature and at elevated temperature, were used in References 1-3 and 1-4 to show that no correlation exists between loss coefficient and contact pressure. However, because the data exhibit considerable scatter, confidence in this data analysis was low. Engineering judgment could suggest that loss coefficient might be related to the absolute contact pressure between the tubes and the tubesheet. Hence, a requirement was applied to the H* leakage analysis by the regulatory authorities that it is necessary to show that the contact pressure at accident induced conditions exceeds the contact pressure at normal operating conditions (Pc_{SLB}:Pc_{NOP}>1).

The calculated contact pressure results for all models of SG are, to a large degree, dependent on the temperatures at a particular operating condition. The limiting accident leakage condition for H* for the Model D5 SGs is the feedwater line break (FLB) condition. However, the limiting accident condition for the structural analysis of the Model D5 SGs is the steam line break (SLB) condition. The licensing basis for the Model D5 SG includes a SLB condition that differs from the SLB conditions in the licensing basis for the other SG models. The Model D5 SG SLB transient includes a significantly lower temperature; as a result, it cannot be shown that the contact pressures at accident conditions exceed those at normal operating conditions, and the criterion for contact pressure (Pc_{SLB}:Pc_{NOP}>1) is not met in application of the C^2 model as well as the SF model. Consequently, it was necessary to utilize a different approach for leakage analysis that does not depend on loss coefficient being independent of contact pressure to show that the accident induced leakage value assumed in the FSAR is not exceeded. Two alternate leakage methods were discussed in Reference 1-11.

1.2.3 C^2 Model Contact Pressures Results

Although in general, the C^2 model contact pressure results exceed those based on the scale factor (SF) model results, the contact pressure results based on the C^2 model are not always greater than the scale factor (SF) model results. Using the C^2 Model, it was determined that the magnitude of contact pressures did not increase at all tubesheet radii at all elevations relative to the SF analysis results during normal operating and SLB conditions. As a result of the change in contact pressures, re-calculation of the probabilistic H* value was required for each model SG in the H* fleet.

1.2.4 Process for Determining the Limiting H* Value

The final H* depth recommended is the 95% probability at 50% confidence (95/50) estimate of H*. Consistent with prior practice, the 95% probability at 95% confidence (95/95) estimate of H* is also provided for information. The probabilistic H* depth is based on the mean H* value for the limiting tubesheet radius. When applying the C^2 model, the definition of the mean H* must include an adjustment for Poisson contraction because the model does not inherently include it. The thick shell model inherently included the effect of Poisson contraction. Poisson contraction is a physical property of the material and, therefore, must be accounted for in the calculation of the H* values. Calculation of the mean H* value is required to determine the radial location on the tubesheet at which to calculate the probabilistic values of H*; however, the calculation of the probabilistic H* is independent of the mean value of H*. Including the Poisson contraction when determining the mean value of H* is important insofar as the radial location of the limiting mean value of H* may depend on application of the Poisson correction.

As discussed in detail in References 1-3 and 1-4, the principal variables affecting the probabilistic value of H* are the coefficients of thermal expansion of the tube and tubesheet materials. The specific values of these variables that define probabilistic analysis of H* based on the C^2 model are determined from the variability surface described in Figure 8-5 of References 1-3 and 1-4. Application of these values in the C^2 model is discussed in Section 3.4 of this report. The probabilistic estimate of H* is further adjusted by the addition of a factor to account for the Poisson contraction of the tubes due to end cap loading, and a further adjustment of the length to account for the effect of the crevice pressure distribution which is dependent on the initially predicted length of H*. The adjustment for crevice pressure distribution is discussed in References 1-3 and 1-4 and Section 3.4 of this report. The adjustment for Poisson contraction is discussed in Section 3.5 of this report.

The limiting H* estimate for NOP, SLB and FLB is determined for the worst-case sector of the tubesheet, which is the region of the tubesheet perpendicular to the tube lane, plus or minus five degrees azimuthally (see Section 6.2.3 of References 1-3 and 1-4). The H* estimate is determined using TS displacements from the worst-case sector calculated using a three-dimensional (3-D) half-symmetry finite element model of the lower SG complex described in Section 6.2.1 of References 1-3 and 1-4 and further discussed in Section 3.2 of this report. The tubesheet displacements are input to the calculation of contact pressure between the tube and the tubesheet at multiple elevations at each tubesheet radius in the limiting sector. The distribution of contact pressure as a function of elevation at a given tubesheet (TS) radius (see Section 3.3) defines the pull out resistance of a SG tube to an applied end cap load at that radius. The required H* length is defined by the integration of the cumulative pull out resistance as a function of depth in the tubesheet. The structural model used to calculate the contact pressures between the tubesheet and the tube is a pseudo sub-model to the 3-D FEA model, called the square cell model (C^2 in this report). The C^2 model which is a quarter symmetry model of the tube and tubesheet material in a single tube pitch subjected to applied pressure and temperature in addition to the applied displacements from the tubesheet. A separate C^2 model is developed for each elevation at a single TS radius. The radial location of the worst case H* estimate is the TS radius with the longest required engagement length to balance an end cap load of $3\Delta P_{NOP}$ or $1.4\Delta P_{DBA}$ (whichever condition results in a greater H* value) assuming mean material properties. See Section 3.3 of this report for a detailed description.

The probabilistic estimate of H* is based on a Monte Carlo simulation for determining the effect of varying the TS coefficient of thermal expansion (CTE) and the tube (T) CTE on the contact pressure based on the limiting operating condition from the mean material estimate of H*. The final result of the simulation is the combination of TS and T CTE that defines the 95 percentile probability at a 50 percent or greater confidence estimate for increasing H* during the limiting operating condition at the limiting TS radius. The predicted combination of CTEs from the simulation is input to the C^2 model to calculate the value of H* at the required probabilistic estimate. See Section 3.4 of this report for a detailed description.

The distribution of contact pressure for the limiting operating condition, at the limiting TS radius, at the required probabilistic estimate, is used to determine the effect of Poisson contraction on the probabilistically defined H* value. The effect of Poisson contraction is determined by using standard thick shell equations (see Section 3.5) to calculate the reduction in contact pressure from a corresponding reduction in the outer diameter of the tube due to an applied axial end cap load on a closed thick walled pressure vessel. The net result is added to the probabilistic H* value to increase the required engagement length of the tube portion within the tubesheet. The Poisson contraction is based on the probabilistic

contact pressure profile because the probabilistic value of H* is the basis of the requested license amendment.

The crevice pressure effect is added to H* after the probabilistic value of H* with the Poisson effect is determined. The effect of crevice pressure on the structural analysis is described in Sections 6.4.8 and 8.1.2 of References 1-3 and 1-4 and in Section 3.6 of this report. The crevice pressure adjustment is applied after the adjustment for Poisson contraction because the Poisson contraction is an adjustment for a loading condition that is independent of the crevice pressure correction.

As a result of the issues discussed above, the action plan shifted from demonstrating the conservatism of the current licensing basis to the following:

1. Using the more accurate C^2 model to confirm that the contact pressures at accident conditions exceed those at normal operating conditions, and to demonstrate that the criterion for contact pressure (SLB:NOP>1) for each of the model SGs in the H* Fleet is met at all tubesheet bundle radii. For the Model D5 SG and for the 2 loop Model 44F SG, it was determined that the requirement $Pc_{SLB}:Pc_{NOP}>1$ could not be met; therefore, two alternate means were developed to demonstrate that the leakage factors in place in the current licensing basis remain conservative for these model SGs.

2. Using the more accurate C^2 model, calculation of revised probabilistic H* values for each of the models of steam generators in the H* fleet.

Three reports are provided for the entire population of H* candidate plants:

- WCAP-17330-P, Rev. 1; a combined report for the Model F and D5 SGs (e.g., this report). This report addresses the C^2 model results for the Model F and D5 SGs and provides a final response to RAI Question Numbers 5 and 12. The remainder of the NRC RAI has been answered in previous submittals as discussed in Section 1.2.1 above.

- WCAP-17345-P, Rev. 2, a combined report for the Model 44F and 51F (3-loop plants).

- WCAP-17378-P, Rev. 0, a separate report for the single Model 44F 2-loop plant.

1.3 SUMMARY OF THE IMPACT OF INDEPENDENT REVIEW ON H*

The H* utilities contracted MPR Associates to perform an independent review of the H* analysis that serves as the bases for the permanent alternate repair criteria (PARC). The MPR review recommended three significant changes to the document:

Westinghouse should update the Poisson contraction calculation process.

Westinghouse should provide an improved justification of the simplified C^2 model probabilistic analysis ("breakline" concept).

Westinghouse should add a discussion of the method to transform the 95/50 to 95/95 H*value to the report.

Item No. 1 is discussed in Section 3.5.4, "Calculation of Contact Pressure Reduction from Poisson Effect" of this report. Item Nos. 2 and 3 are discussed in Section 3.4.2, "Methods Discussion" of this report. Also, two new references were included in the report as a result of the MPR review, References 3-16 and 3-17. These references provide an alternate method of justifying the "breakline" concept and an improved statistical analysis of the coefficient of thermal expansion data used in the H* analysis.

It is important to note that the recommendations by MPR Associates did not alter the H* distances or leakage factors identified by Westinghouse in the H* licensing basis documents.

1.4 REFERENCES

1-1. USNRC Letter, "Vogtle Electric Generating Plant, Units 1 and 2, Issuance of Amendments Regarding Technical Specifications (TS) Section 5.5.9, "Steam Generator Program," and TS 5.6.10, "Tube Inspection Report," for Interim Alternate Repair Criteria (TAC Nos. ME1339 and ME1340)," September 24, 2009. (typical for H* participants).

1-2. USNRC Letter, "Vogtle Electric Generating Plant, Units 1 and 2 – Transmittal of Unresolved Issues Regarding Permanent Alternate Repair Criteria for Steam Generators (TAC Nos. ME1339 and ME1340)," November 23, 2009.

1-3. WCAP-17071-P, Rev. 2, "H*: Alternate Repair Criteria for the Tubesheet Expansion Region in Steam Generators with Hydraulically Expanded Tubes (Model F)," September 2010.

1-4. WCAP-17072-P, Rev. 0, "H*: Alternate Repair Criteria for the Tubesheet Expansion Region in Steam Generators with Hydraulically Expanded Tubes (Model D5)," May 2009.

1-5. SM-94-58, Rev. 1, "Doel 4 Elevated Tubesheet Sleeve – ASME Code Evaluation and Effect of Tubesheet Rotations on Contact Pressures," December 1995. (Proprietary)

1-6. LTR-SGMP-10-78 P-Attachment, "Effects of Tubesheet Bore Eccentricity and Dilation on Tube-to-Tubesheet Contact Pressure and their Relative Importance to H*," September 2010.

1-7. LTR-SGMP-10-33 P-Attachment, "H*: Response to NRC Questions Regarding Tubesheet Bore Eccentricity," September 2010.

1-8. USNRC Letter, "Vogtle Electric Generating Plant – Audit of Steam Generator H* Amendment Reference Documents (TAC Numbers ME3003 and ME3004)," July 9, 2010.

1-9. CN-SGDA-03-119, Rev. 1, "Calculation of Loss Coefficient for Model D5 Steam Generators," Westinghouse Electric Company LLC, June 2004.

1-10. STD-MCE-03-49, "Determination of Model D5 Tube-to-Tubesheet Leakage Resistance for H-Star Program for CBE/CDE/DDP/TCX," November 4, 2003.

1-11. LTR-SGMP-10-95 P-Attachment, Rev. 1, "H*: Alternate Leakage Calculation Methods for H* for Situations When Contact Pressure at Normal Operating Conditions Exceeds Contact Pressure at Accident Conditions," September 2010.

2 SQUARE CELL (C^2) MODEL ANALYSIS

This section provides a generic description of the C^2 model. Although there are SG model-specific applications of the C^2 model, the description of the C^2 model is based principally on the application for the Model D5 steam generators because the model was initially developed for the Model D5 steam generators. The entire generic description of the C^2 model applies equally to the Model F steam generators.

2.1 PURPOSE OF THE C^2 ANALYSIS

Figure 1-1 in the current licensing basis (Reference 2-1) defines the calculation process for H*. The foundation for all of the structural analyses is a global model of the lower tubesheet complex (called the 3-D FEA model) that provides the tubesheet displacements that are used to calculate tube-to-tubesheet contact pressures. In the current licensing basis for H*, based on the thick shell equations, tubesheet displacements generated by the bending of the tubesheet from the primary-to-secondary pressure differential in the global 3-D model are applied directly to the inner diameter of the tubesheet tube bore. This is a very conservative assumption that does not accurately represent the real physical condition.

The deflections of the tubesheet tube bore surfaces occur due to the radial thermal growth, radial pressure growth and the primary-to-secondary pressure differential acting on the tubesheet. The thermal growth of the tubesheet itself and the distortion of the tubesheet tube bore due to bending of the tubesheet under the primary-to-secondary pressure differential are transmitted to the tube bore through the tubesheet material to the ligament surrounding a given tube. The square cell model analysis (C^2) is a more accurate approach to modeling the process by which the tubesheet deformations are transferred to an individual tube bore. Figure 2-1 and Figure 2-2 illustrate the differences between the approach utilized in the thick shell model and that used in the square cell model in applying the displacement calculated with the 3-D FEA lower tubesheet complex model.

In Figure 2-1, the calculated local displacements are applied to the inner diameter of the tubesheet tube bore. In Figure 2-2, the calculated local displacements are applied to the outer edges of the tubesheet cell material, and the displacements at the inner diameter of the tubesheet tube bore evolve from the local structural model (the C^2 model). The analysis method in Figure 2-2 is physically more realistic because it mimics the process by which the gross tubesheet displacements are transferred to the circumference of the tubesheet tube bore. The analysis method in Figure 2-1 is the simplest option for comparing the finite element model to analytical equations, i.e., the classical thick shell equations. Also, if the geometry of the model is circular, the simplest way to apply a postulated load or displacement on the collars is to a surface which includes the inner diameter. However, because the global model does not include a distinct representation of the individual tube bore, additional assumptions must be made to determine what displacements should be applied to the boundaries of a local model (as shown in Figure 2-2) so that the tubesheet tube bore deflects in a realistic fashion.

The issue of how tubesheet tube bore deflection affects the tube-to-tubesheet contact pressure is the same regardless of the method chosen to apply displacements from the large scale model (3-D FEA) to the local sub-model. The basic problem is defined by how the large scale tubesheet deflections are transferred (or "mapped") to the local scale of a single tubesheet tube bore and tube. For the purposes of this report, the terms large scale and global scale refer to the 3-D finite element model of the channelhead, tubesheet,

divider plate and lower shell (a.k.a., "stub barrel") that make up a typical Westinghouse designed steam generator in the existing domestic fleet (see Figure 2-3). In the case of the prior H* analysis (Reference 2-1), the sub-modeling is complicated by the fact that the presence of the perforations in the tubesheet are smeared throughout the perforated region in the tubesheet using the method of Slot (Reference 2-2). This means that in the global model of the lower steam generator complex the tube bores do not exist although the effect of the perforations on the structure is accounted for with respect to pressure and temperature. This is a complication for the square cell model approach because the exact displacements around a tube pitch cannot be directly taken from the 3-D finite element model of the lower SG complex.

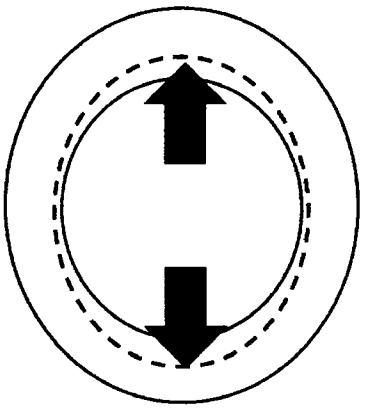

Figure 2-1 Current Licensing Basis Tubesheet Bore Displacements
(Local displacement applied directly to tubesheet bore)

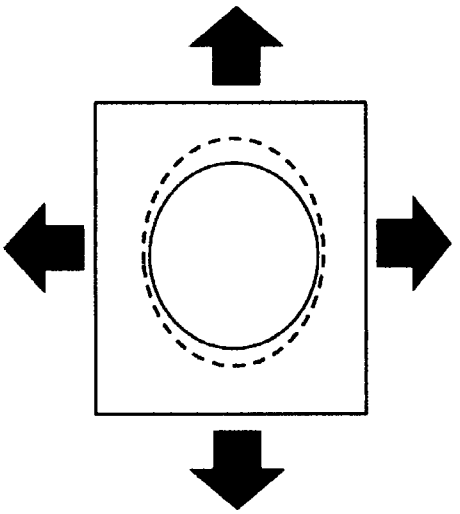

Figure 2-2 C^2 Model Tubesheet Bore Displacements
(Local displacement applied to surrounding tubesheet material)

The effect of the perforations in the non-perforated model with the effective material properties includes the expansion of the tubesheet with respect to temperature and pressure, assuming that all the tubes in the bundle are pressurized. The elastic modulus and Poisson's ratio of the perforated material are altered so that the isotropic material becomes orthotropic. This means that the stiffness of the tubesheet along different axes is different so that the expansion of the tubesheet due to the combined pressure and temperature loads is conserved without the perforations being modeled. The question remains as to how to include the effect of the individual tube bores interacting locally. That question can be accommodated using different sub-models which, in general, are not necessary to calculate the tube-to-tubesheet contact pressure. Section 6.2.3 in Reference 2-1 describes one approach to bridging the gap between a single tubesheet tube bore in an isolated model and including effects for the presence of other linked tubesheet tube bore at a local scale due to pressure at a given operating temperature. The reason they are not necessary is that along any given radial line from the center of the tubesheet it is possible to determine what the displacement is over that entire distance. This means that the displacement of a unit section can be determined but the displacement of a specific tube bore cannot be determined from the global model. In the case of H*, the displacement of specific tubes at key radii is used in determining the average tube-to-tubesheet contact pressure.

Figure 2-3 shows a general model of the lower steam generator complex which is the source of the displacements used in the square cell analysis. The intent of the C^2 model is to simulate a limited thickness "core sample" of a single tube at a given radius as shown in Figure 2-4. The square cell model, shown in Figure 2-5, Figure 2-7, and Figure 2-8, is a local model consisting of plane stress solid elements that approximate the tube and tubesheet material defined by a one-half tube pitch around a single tubesheet tube bore through the thickness of the tubesheet (typically 21.03 inches). This is the definition of the unit "square cell" model of the local tubesheet tube bore. The intent of this model is to provide a physically more realistic estimate of the contact pressure between the tube and the tubesheet at various elevations through the thickness of the tubesheet during the operating condition of interest.

2.2 DEFINITION OF THE C^2 MODEL

The square cell model is based on a unit cell of tubesheet material surrounding a single tubesheet tube bore in various models of Westinghouse steam generators. Each SG model is represented by a separate square cell model. The square cell is defined by taking one-half of the nominal tube pitch around a tube as the limit of the material in the model. The initial dimensions for the square cell model are based on the room temperature unpressurized condition. For example, in a Westinghouse Model D5 SG, the tube pitch is [ ]^{a,c,e} inches. The outer nominal tube radius is [ ]^{a,c,e} inch. The inner nominal tube radius is [ ]^{a,c,e} inch. The resulting square cell is shown in Figure 2-7 below, with typical boundary conditions applied on the model. A quarter section of the model is typically used for analysis.

The square cell model is oriented in the X-Z plane of the tubesheet as defined in the lower SG complex shown in Figure 2-3. (For clarity, the square cell model is in the plane of the tubesheet but, for convenience, the square cell model is imported to *ANSYS* in an X-Y plane as noted in Figure 2-6.) The applied displacements, or forces, representing the net strain over the cell in the global X direction (formerly referred to in prior RAI responses as "e-bar") and the global Z direction (formerly referred to in prior RAI responses as "z-bar"). These net displacements are now referred to as ΔX and ΔZ.

a,c,e

Figure 2-3 Typical Lower SG Complex Model

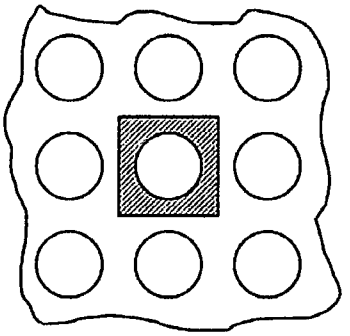

Figure 2-4 Square Cell Model "Core Sample"

a,c,e

Figure 2-5 Square Cell Model

a,c,e

Figure 2-6 Typical Square Cell Coordinate System

a,c,e

Figure 2-7 Typical Square Model without Symmetry Conditions

a,c,e

(a) Coarse Mesh

a,c,e

(b) Fine Mesh

Figure 2-8 Typical Mesh Square Cell with Quarter Symmetry Conditions

2.3 APPLICATION OF BOUNDARY CONDITIONS

There are three categories of boundary conditions that are applied in the square cell model: thermal, pressure and displacement. All components in the square cell model are assumed to be at a uniform temperature, depending on the operating condition, with the tube in equilibrium with the primary fluid temperature. The approaches taken in this analysis were selected because they are consistent with the current licensing basis for H*. The discussion below summarizes the issues with each approach to applying the pressure and displacement loads to the square cell model. The impact of any installation effects from the hydraulic expansion of the tube into the tubesheet tube bore is ignored in this analysis in order to be consistent with the licensing basis used for H*. The potential effect of any strain-hardening from the expansion process can be ignored because the calculated elastic stresses in the tubes do not exceed the elastic limit of the tube material (see Section 6.2.5 of Reference 2-1).

2.3.1 Deformation of Tubesheet Cell Edges

Displacement based boundary conditions are used in the C^2 approach in a pseudo sub-model approach because the global model dictates how the sub-model should behave at the nodal level. For example, if the displacements due to the effect of temperature and pressure around the entire boundary of the sub-model are known, then those displacements can be directly applied to the sub-model. The square cell analysis is not a true sub-model analysis because the nodal displacement is not used as the applied boundary conditions. Instead, the average displacements over a tube pitch at a specified location and elevation are used. Loads which lead to additional displacements in the C^2 model (such as the thermal expansion of the tubesheet tube bore inner diameter) are not additive with the displacements from the initial conditions taken from the global SG model. This is because the applied displacements on the boundaries of the square cell model already account for the expansion of the tubesheet material due to pressure and temperature.

The preferred approach in the square cell analysis is to specify displacements at the boundaries of the tubesheet material as taken from the 3-D finite element model of the lower SG complex. Figure 2-9 illustrates the potential responses to the applied displacement that can occur in the square cell model.

It is important to understand that from the perspective of calculating the tube bore eccentricity based on the deflection of the major and minor axes of the tube bore all of the possibilities in Figure 2-9 (a through c) are equal. The reaction of the model to those displacements is different based on how the nodal constraints are applied. For example, in Figure 2-9a, all nodes on the boundaries are assumed to expand equally along the different axes. In Figure 2-9b, nodal constraints are used so that the end points of the tubesheet material deform the entire distance and the remainder is linearly related to the maximum displacement. In Figure 2-9c, the displacement of the two surfaces in the model develops naturally based on the applied displacement with no constraints on the nodal behavior. Figure 2-9a is the most conservative application of the displacement because it minimizes contact forces. Figure 2-9b tends to maximize the eccentricity in the tubesheet tube bore. It is not physically possible for the outer edges of the tubesheet material to deform in this manner because a stress discontinuity will result at the intersections of the orthogonal boundaries. Further, the growth from adjacent pressurized tubesheet tube bore will also act to prevent such a deformation in the majority of the bundle. Figure 2-9c has no assumptions on the deformation of the tubesheet tube bore material and allows a non-uniform displacement to develop on either edge in response to the applied displacement. However, the majority of

the deformation in the tubesheet is due to thermal effects, which means that the tubesheet material should deform in a mostly uniform manner. Therefore, the approach shown in Figure 2-9c is not used. Figure 2-9a is the preferred approach to applying the displacement taken from the lower SG complex model because it is the most conservative for calculating H*.

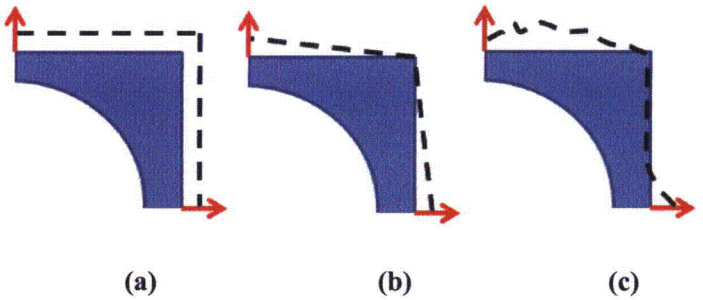

Figure 2-9 Sketches of Possible C^2 Model Response to Applied Displacement

2.3.2 Applying the Internal and Crevice Pressures in the Square Cell Model

Two pressure loads must be accounted for in the square cell model. The first is the internal pressure acting on the inner diameter of the tube representing the reactor coolant pressure. The second is the crevice pressure that the outer diameter of the tube and the inner diameter of the tube bore are exposed to assuming a through-wall flaw in the tube. The distribution of the crevice pressure varies according to the elevation of the tube in the tubesheet relative to the location of the flaw that allows the primary coolant into the crevice (References 2-3 and 2-4).

The internal pressure and crevice pressure can be included in the square cell model in two ways: First, the difference in the pressure acting on the outer diameter of the tube and the inner diameter of the tube can be applied as a pressure load that varies according to the elevation within the tubesheet. In this case, both the internal pressure acting on the tube and the crevice pressure are combined into the single differential pressure applied on the inner diameter of the tube. Second, the full internal pressure is applied to the inner diameter of the tube and the full crevice pressure (as a function of elevation) is applied to the outer diameter of the tube and the inner diameter of the tubesheet tube bore. The first option is the preferred approach in the square cell model because it conservatively minimizes the growth of the tube at the lower elevations of the tubesheet. This leads to a reduced contact pressure at the bottom of the tubesheet. This option is also simple to resolve with the contact options available in the structural analysis code, *ANSYS*, because a uniform pressure is pushing the outer surface of the tube into the inner surface of the tubesheet. The second crevice pressure option is difficult to resolve with the contact options in *ANSYS*.

The crevice pressure is assumed to act on 100% of the circumference of the outer diameter of the tube surface and inner diameter of the tubesheet tube bore. It is also simpler to account for the effect of the crevice pressure over the entire tubesheet tube bore as opposed to limited regions of the tube outer diameter. This assumption is conservative because test data (References 2-1 and 2-4) shows that this cannot occur. The observed leakage during the tests was more aptly characterized as "weepage," i.e., dropwise leakage. Also, recent work reported in the literature (Reference 2-5) based on fluid structure interaction shows that fluid blanketing of the entire crevice cannot occur. Both point to evidence that

supports the assumption in the analysis of record for H* of a "tortuous path" that the liquid must take as it diffuses through the porous medium of the tube-to-tubesheet crevice. However, the nature of the test specimens, used in References 2-1 and 2-4, make it impossible to ascertain what portion of the tube outer diameter constitutes a wetted surface. Limited sensitivity studies have been performed to determine the effect of applying the crevice pressure over a smaller portion of the tube. In these studies, "bubbles" of crevice pressure were applied to the tube bore inner diameter and the tube outer diameter while the full internal pressure was applied to the inner diameter of the tube. The "bubbles" varied in circumferential extent from 10 to 75 percent of the tube outer diameter. The effect of limiting the crevice pressure to less than 100 percent of the outer tube diameter was an increase in the average tube-to-tubesheet contact pressure of at least 10 percent.

2.4 MATERIAL PROPERTIES

The manufacturing process used to assemble a steam generator creates a strain-hardened condition in the tubes. The tubes are initially inserted into the steam generator tubesheet tube bores, "tack" expanded into the tubesheet near the tube end by hydraulic (urethane plug) expansion or mechanical hard rolling over approximately a 0.75 inch length, and welded to the tubesheet. Each tube is then hydraulically expanded into contact with the tubesheet tube bore over the full depth of the tubesheet. This means that each of the tubes in the tube bundle begins in contact with the tubesheet tube bore. It also means that the tubes create a material non-linearity with respect to the contact pressure analysis because they are strain-hardened to a small percentage (1 to 3 percent on average) and typically thinned to a small extent (~1% wall thinning) [Reference 2-1]. No non-linear material effects are present in the tubesheet tube bore material. Consistent with the basis of the current licensing basis, the square cell model ignores any effects that could benefit the contact pressure analysis that come from the tube installation and steam generator manufacturing process, including any strain-hardening effect, residual contact pressure, wall thinning or other material non-linearity.

Test data has shown that the installation and tube expansion process develops sufficient pull out resistance between the tube and the tubesheet at room temperature and at elevated temperature conditions (Reference 2-1) to resist any applied pull out loads during normal and accident conditions. Any additional contact pressure due to tubesheet deformation or applied pressure is above what is already sufficient to prevent pull out of the tube portion within the tubesheet. Therefore, it is conservative and convenient to ignore strain-hardening resulting from initial tube expansion as an initial condition. No elastic-plastic effects are included in the analysis. The displacements and pressures acting on the tubes are applied in an elastic analysis. This is appropriate provided that the average radial stress in the tube material due to the applied loads is less than [ ]^{a,c,e} ksi. None of the contact pressure results in the tube material for the square cell model described in this report approached an average radial stress of 30 ksi.

The material properties used for the tube and the tubesheet materials in square cell model are the same as originally used in the licensing basis analysis, Reference 2-1. The properties used for the Alloy 600 thermally treated tubing and SA-508 tubesheet materials are provided in Table 3-3 and Table 3-4.

The Poisson's Ratio used for the tube material is 0.28[1]. The Poisson's Ratio used for the tubesheet material is 0.30.

2.5 CONTACT MODELING DISCUSSION

The only boundary conditions that limit the displacement of the tube in the square cell model are the symmetry conditions on the edges of the model. This means that in the square cell model the contact between the tube and the tubesheet is what limits the potential displacement of the tube. If the contact relationship between the tube and the tubesheet is modeled inappropriately, the tube in the model could slide past the tubesheet and experience rigid body translation. Another possibility is that the tube deformations could lead to inter-penetration of the tube material into the tubesheet material which would generate unrealistically high contact pressures. Conversely, if the contact law is determined to resist node-to-node contact too strongly, the results of the analysis would be an unrealistically low contact pressure. While the *ANSYS* solver is capable of using different numerical schemes to resolve these difficulties, it is up to the user to make sure that the results which are obtained are appropriate. In the application of the square cell model, the contact pressure results using different contact modeling options were compared to determine the best approach. The final contact model used in the square cell analysis is a frictional model which is consistent with the assumptions in the H* analysis (e.g., μ = [ ]^{a,c,e}).

In FEA structural modeling, the simplest way to prevent difficulties with a contact law is to construct a properly converged mesh. The metric used for mesh convergence in the C^2 analysis is the average contact pressure (radial stress) between the tube and the tubesheet. A mesh is typically considered properly converged when the change in the average contact pressure from a model with an increased mesh density is less than a defined percentage (i.e., 2%) different from the prior mesh density. It is difficult for nodal interpenetration to occur if a mesh is fine enough, because the nodes on either side of the contact surface will be aligned and cannot "slip" past each other. The symmetric boundary conditions also help to maintain the nodal positions on either side of the contact surface so that the nodes remain aligned properly throughout the analysis. Several mesh designs were evaluated in the C^2 analysis. Figure 2-8 shows the coarsest and the finest meshing schemes used in the analysis. The coarse mesh (shown in Figure 2-8a) has approximately [ ]^{a,c,e} contact elements along the tube-to-tube bore interface. The fine mesh (shown in Figure 2-8b) has approximately [ ]^{a,c,e} contact elements along the tube-to-tube bore interface.[2] The finer meshing schemes tend to predict an increase in the tube-to-tubesheet contact pressure relative to the coarser meshes and can resolve the contact pressure closest to the boundaries in a quarter symmetry model with a higher degree of accuracy. However, the contact pressures nearest the displacement boundary conditions on the tube in the quarter symmetry model are not significant to the problem and lower contact pressures are conservative. Therefore, for conservatism, the preferred meshing scheme in the square cell analysis is a slightly more coarse mesh. Tests of the coarser mesh showed that it

1. The 2007 Edition of the ASME Code gives a value of Poisson's Ratio for Alloy 600 as 0.31. This is used in the Poisson's Ratio contraction calculation (Section 3.5) because that calculation focuses solely on the tube material. A Poisson's ratio of 0.28, a 10% reduction in the Code value and within the stated potential variation of the ASME Code properties, is used for the tube in the square cell analysis in order to facilitate the finite element analysis. Reducing the Poisson's ratio of the tube in this case increases the difference in the stiffness coefficients between the tube and the tubesheet which reduces the likelihood of numerical complications due to stress singularities in the model. The net effect on the calculations from using a Poisson's ratio of 0.28 for the tube is a slight reduction (conservative) in contact pressure, on the order of 10 psi, compared to using the ASME Code value of 0.31 for Poisson's ratio.

2. The final meshing scheme used in the C^2 results described in this report for the calculation of H* has approximately [ ]^{a,c,e} contact elements along the tube and tubesheet interface.

was sufficiently fine to prevent nodal interpenetration. The actual mesh used in the final analysis is shown in Figure 3-13.

The C^2 model mesh was converged to within a 2% difference of the previous model, at which point it was judged that additional refinement of the mesh would not yield a sufficient increase to merit the additional computational effort to solve the model. At that point, the model mesh refinement was reduced to the level of a 5% difference (equating to a roughly 3% reduction in contact pressure from the fine mesh model results) in the average radial stress along the outer diameter of the tube in order to reduce the amount of time necessary to perform each analysis. The alignment of the nodes on both the tubesheet surface and the tube surface was maintained by the boundary conditions in the model so that regardless of what level of mesh refinement was used they would line up appropriately and prevent fictitious material interpenetration.

The potential for an artificially stiff interface between the tube and the tubesheet was addressed in the square cell model. In the *ANSYS* model used for the analysis, the augmented Lagrangian contact model allows a user to specify the interfacial normal stiffness (any value between 0.01 and 10) or to have the computer determine it automatically in the course of calculating the solution to the model. In the square cell analysis, a sensitivity study was done using the converged mesh in which the solution for the interfacial stiffness was determined by the computer. The result of that study showed that the initial interfacial normal stiffness began at 1.0 and varied between 0.7 and 1.2 at the end of the solution. These values resulted in material penetrations on the order of 10^{-9} to 10^{-13} inch, with very little change in the resulting contact pressure. A non-varying value of 0.7 is used for the interfacial normal stiffness in the square cell analysis which results in interpenetrations on the order of 10^{-9} to 10^{-10} inches. This small level of interpenetration is not a significant issue and is within the bounds of calculated error in the solution process using the *ANSYS* solver. The interfacial normal stiffness is fixed in order to facilitate the numerical solution of the model.

The tubesheet is defined as the contact target body because the deformation of the tubesheet material is more controlled. The tube is defined as the contact body because the tube is expanding into the tubesheet material and its deformation is poorly controlled in the model. The contact relationship between the tube and the tubesheet is defined as symmetric and rough (e.g., with friction). The contact is symmetric for numerical expediency and because, in the range of deformations under consideration, the tube may lose contact with the tubesheet or the tubesheet may lose contact with the tube. The friction interface allows two-dimensional sliding between the tube and the tubesheet. Shear stresses can develop due to "stick-slip" behavior because the coefficient of friction between the tube and the tubesheet in this model is greater than zero. However, these shear stresses are separate from the calculated contact pressures in *ANSYS* and do not affect the final results used to calculate H*.

The augmented Lagrangian solver in *ANSYS* is used to resolve the contact so that the contact pressure results have a smaller variation around the circumference of the tube bore and because the extra degree of freedom helps the solver to calculate the contact interactions quickly. The tube and tubesheet are initially adjusted to be "just touching" using the contact options in *ANSYS*. The geometry defined in the model is such that the tube and tubesheet begin in line on line contact at the tube-to-tubesheet interface. However, the possibility exists for a small geometric inconsistency to lead to an interpenetration of the tube and tubesheet materials. Therefore, the tube outer surface and tubesheet inner surface are separated by an

initial offset of +0E00 inch in *ANSYS* to set the initial gap to zero and to assure that no interpenetration occurs.

There are two options used in the analysis for managing the stiffness of the interface in the square cell model. The first option assumes that the stiffness of the interface is constant and does not need to be updated as the analysis proceeds to completion. This first option is the most similar to an analytical model using thick shell equations to solve for the contact pressure between the tube and the tubesheet. The second option assumes that the stiffness must be constantly updated to prevent interpenetration of the tube and tubesheet and adjust the contact law as the deformation of the nodes at the interface shift during the analysis. The "pinball" radius was set to [ ]^{a,c,e} inch to reflect the surface roughness of the post-expanded tube. The pinball radius is the distance about a node on a defined contact surface which, if another existing node on a defined contact surface is equal to or closer than, the two surfaces are recognized to be in contact with each other.

2.6 DISCUSSION OF BENCHMARK MODEL FOR C^2 MODEL COMPARISON

The contact pressure results for the square cell analysis were benchmarked against classical thick shell equations. The thick shell model for the composite tube and tubesheet collar was developed to accept the displacement of the tubesheet inner diameter surface as input. The benchmark model used the Model D5 tube and tubesheet geometry. The benchmark model used a different thick shell model (see below) than described in the existing licensing basis for the calculation of the H* analysis contact pressures because the goal of the model was to provide an independent check on the square cell model results and the H* methodology.

2.6.1 Thick Shell Model to Describe Finite Element Model

The tube and tubesheet cylinders can be represented as two concentric, open cylinders. The tube material is thermally-treated Alloy 600. The tubesheet material is SA-508 Class 2. Neither cylinder has an applied axial load. There is no internal pressure within the tube. The coefficient of friction between the inner diameter of the tubesheet and the outer diameter of the tube is zero. The tube and the tubesheet are held at the same constant temperature during the simulation of the operating condition although the tubesheet is assumed to have a coefficient of thermal expansion equal to zero. The tube bore dilation, or expansion of the inner tubesheet collar diameter, is specified in the analysis and assumed to be constant regardless of any applied loading for the tube. The tube and tubesheet cylinders are assumed to have a zero stress, or a constant stress condition, along the tube axis (e.g., $\sigma_{ZZ} = 0$ psi). The assembled model geometry appears in Figure 2-10.

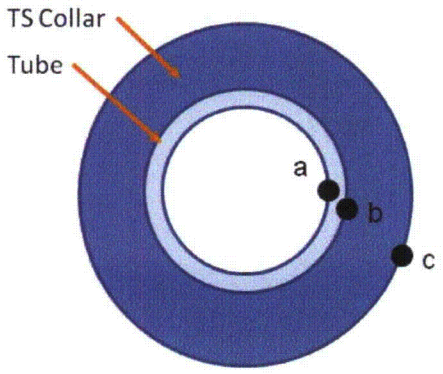

Figure 2-10 Tube and TS Collar Assembly

In Figure 2-10, *a* is the inner radius of the tube, *b* is the outer radius of the tube and also the inner radius of the tubesheet tube bore, and *c* is the outer radius of the tubesheet collar.

The free radial expansion of the tube, due to a change in temperature, is given by:

$$\Delta R_{\Delta T} = \frac{OD}{2} \bullet \alpha_{TUBE}\left(t - t_{REF}\right) \qquad \text{(Equation 2-1)}$$

Where OD is the outer diameter of the tube, α_{TUBE} is the coefficient of thermal expansion of the tube, t is the temperature of the tube and t_{REF} is the reference temperature in the analysis for the material of interest (typically 70°F). Several values of constant tubesheet tube bore inner diameter displacements were selected for the purposes of this sensitivity study. It is assumed that the tubesheet is essentially rigid with respect to any applied loading from the tube in excess of the initial dilation. The tube bore is assumed to deform (or dilate) as a perfect circular surface without any non-uniformities around the circumference of the tube. The difference between the specified tubesheet tube bore dilation and the amount that the tube wants to expand will create a contact stress between the tube and the tubesheet. See Figure 2-11.

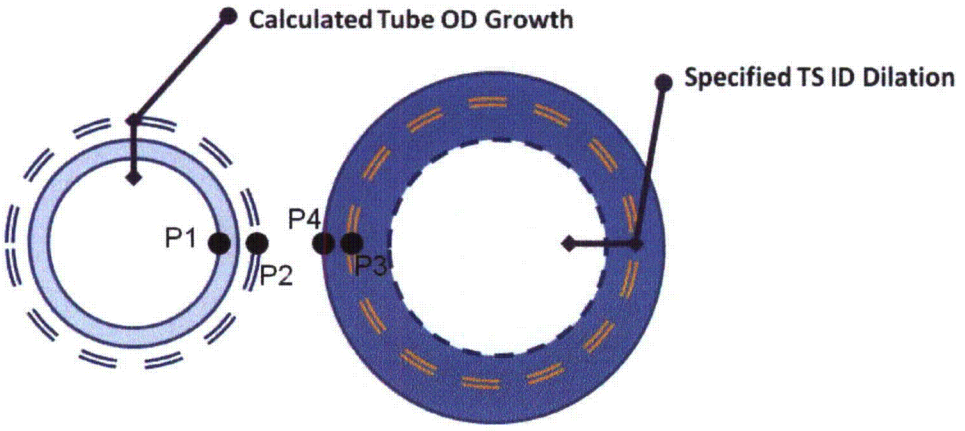

Figure 2-11 Constant Tubesheet Bore Dilation Model

In Figure 2-11, P1 is the internal pressure applied to the inner surface of the tube, P2 is the external pressure applied to the outer surface of the tube, P3 is the internal pressure applied to the inner surface of the tubesheet collar, and P4 is the external pressure applied to the outer surface of the tubesheet collar. In the tube and tubesheet assembly, the contact pressure between the two cylinders is taken at the inner surface of the tubesheet collar and the outer surface of the tubesheet such that they are both equivalent (e.g., P2 = P3). There are no other applied pressures on the system so P1 = P4 = 0 psi.

The differential free radial expansion of the tube at normal operating conditions (NOP, t = [ ]^{a,c,e} °F) and steam line break conditions (SLB, t = [ ]^{a,c,e} °F), calculated using Equation 2-1 and the material properties defined in Table 3-3 and Table 3-4. The NOP operating temperature of [ ]^{a,c,e} °F was chosen to better compare to previous results in Reference 2-1 and is still representative of typical NOP conditions. The results are summarized in Table 2-1.

The difference between the inward radial dilation of the tubesheet tube bore and the outer diameter of the tube will change based on the temperatures during operation. The difference between the specified radial dilation of the tubesheet tube bore and the radial growth of the tube for each operating condition is shown in Table 2-2.

Column (1) in Table 2-2 is the assumed inner radius of the tubesheet tube bore and Column (2) in Table 2-2 is the amount that the tubesheet tube bore is allowed to dilate in the analysis. Column (3) and Column (4) in Table 2-2 are the difference between the allowed dilation in Column (2) and the results in Table 2-2 for each operating condition (e.g., ΔU_{NOP} = Tube Growth – Tubesheet Growth). The difference between the deformations is taken so that a positive value means that the tube deformation exceeds the growth allowed by the tubesheet collar.

The equation for the radial deformation (either positive or negative) of the tube as an open thick walled cylinder at a constant temperature due to pressure loading is:

$$\Delta R_{TUBE} = \frac{r}{E_{TUBE}\left(b^2 - a^2\right)}\left[\left(1 - \nu_{TUBE}\right)\left(p_1 a^2 - p_2 b^2\right) + \frac{\left(1 + \nu_{TUBE}\right)a^2 b^2}{r^2}\left(p_1 - p_2\right)\right] \quad \text{(Equation 2-2)}$$

Where r is the radial location within the tube material, b is the outer radius of the tube, a is the inner radius of the tube, E_{TUBE} is the Young's modulus of the tube at the given operating condition and ν_{TUBE} is the Poisson's Ratio for the tube material. The equation for the radial deformation (either positive or negative) of the tubesheet collar as an open thick walled cylinder at a constant temperature due to pressure loading is:

$$\Delta R_{TS} = \frac{r}{E_{TS}\left(c^2 - b^2\right)}\left[\left(1 - \nu_{TS}\right)\left(p_3 b^2 - p_4 c^2\right) + \frac{\left(1 + \nu_{TS}\right)b^2 c^2}{r^2}\left(p_3 - p_4\right)\right] \quad \text{(Equation 2-3)}$$

Where r is the radial location within the tubesheet material, c is the outer radius of the tubesheet collar, b is the inner radius of the tubesheet collar, E_{TS} is the Young's modulus of the tubesheet at the given operating condition and ν_{TS} is the Poisson's Ratio for the tubesheet material.

The deformation of the tube is limited by the specified deformation of the tubesheet collar, as shown in Table 2-2, Columns (3) and (4). The values in Columns (3) and (4) are all positive; therefore, the final state of the tube outer surface and the tubesheet inner surface is positive contact. The magnitude of the contact pressure between the tube and the tubesheet will be the result of the additional growth that the tube cannot release due to the "rigid" tubesheet collar. The equation for the change in radial position of the contact surface between the tube and the tubesheet is:

$$\Delta U = [\Delta R_{TS}]_{r=b} - [\Delta R_{TUBE}]_{r=b} \qquad \text{(Equation 2-4)}$$

Where ΔU is the condition specific result from Table 2-2 for the appropriate value of tubesheet collar dilation in Column (2). Setting P1 and P4 equal to zero and P2=P3 in Equation 2-2 and Equation 2-3 yields the following for r = b,

$$\Delta U = \frac{b}{E_{TS}\left(c^2 - b^2\right)}\left[\left(1 - \nu_{TS}\right)\left(p_2 b^2\right) + \frac{\left(1 + \nu_{TS}\right)b^2 c^2}{b^2}\left(p_2\right)\right] - \ldots$$

$$\ldots - \frac{b}{E_{TUBE}\left(b^2 - a^2\right)}\left[\left(1 - \nu_{TUBE}\right)\left(-p_2 b^2\right) + \frac{\left(1 + \nu_{TUBE}\right)a^2 b^2}{b^2}\left(-p_2\right)\right] \qquad \text{(Equation 2-5)}$$

Rearranging to solve for p_2 gives the final result.

$$p_2 = \Delta U\left[\frac{b}{E_{TS}\left(c^2 - b^2\right)}\left[\left(1 - \nu_{TS}\right)\left(b^2\right) + \left(1 + \nu_{TS}\right)c^2\right] + \frac{b}{E_{TUBE}\left(c^2 - b^2\right)}\left[\left(1 - \nu_{TUBE}\right)\left(b^2\right) + \left(1 + \nu_{TUBE}\right)a^2\right]\right]^{-1} \qquad \text{(Equation 2-6)}$$

Solving Equation 2-6 for each value in Column (3) and Column (4) in Table 2-2 with the properties in Table 2-3 and Table 2-4 yields the results shown in Table 2-5.

The results in Table 2-6 exclude any effect of non-uniform deformation around the circumference of the tubesheet tube bore. The loss of contact pressure between the tube and the tubesheet is due solely to the expansion (or dilation) of the tubesheet tube bore relative to the expansion of the tube due to thermal effects. Real deformations applied to the tubesheet tube bore are not perfectly uniform. Therefore, the displacement of the inner tubesheet tube bore was used in order to benchmark the model to compare directly against the C^2 model. Only the average tube-to-tubesheet contact pressure around the circumference of the tube can be calculated using the thick shell equation. This is an acceptable comparison to the finite element results because only the average contact pressure around the circumference of the tube is used in the calculation of H*. This benchmark was performed for the Model D5 NOP condition. The expansion of the inner surface of the tubesheet tube bore due to a pressure differential across the tube wall (i.e., the pressure of the primary fluid minus the assumed circumferentially uniform pressure in the tube/tubesheet crevice) and an applied temperature is shown in Table 2-6. This result was then applied to the inner diameter of the tubesheet surface in the C^2 model. The tube bore displacement in Table 2-6 varies as a function of elevation due to the change in the crevice pressure distribution. The result of using the calculated tubesheet tube bore displacements in the square cell and analytical models is given in Table 2-7. The average contact pressure between the tube and the tubesheet in the C^2 approach with the contact law as described is a very close approximation of the thick

shell equation for the same uniform tubesheet tube bore displacement. Based on the comparison with the thick shell equation models, the C^2 approach and the modeling described in this section are reasonable and appropriate.

Table 2-1 Free Radial Expansion of a Tube

Condition	Nominal Tube OR	α_{TUBE}	T	t_{REF}	ΔR
	in	in/in-°F	°F	°F	in a,c,e
NOP	[				]
SLB	[				]

Table 2-2 Difference between Radial Dilation of the Tube Bore and Tube

(1)	(2)	(3)	(4)
Avg TS IR	Change in TS IR	ΔU_{NOP}	ΔU_{SLB}
in	in	in	in a,c,e
0.3810	[		]
0.3811			
0.3813			
0.3815	[		]

Table 2-3 Rigid Collar Model Input Parameters (Tube)

Nominal Tube Properties			
Variable	Description	Value a,c,e	Units
b	OR	[ ]	in
a	IR		in
	E (NOP)		psi
	E (SLB)		psi
	α (NOP)		in/in-°F
	α (SLB)		in/in-°F
	Poisson's Ratio		-

Table 2-4 Rigid Collar Model Input Parameters (Tubesheet)

Nominal TS Properties			
Variable	**Description**	**Value**	**Units**
c	OR	[ ]a,c,e	in
b	IR		in
	E (NOP)		psi
	E (SLB)		psi
	a (NOP)		in/in-°F
	a (SLB)		in/in-°F
	Poisson's Ratio		-

Table 2-5 Rigid Collar Model Contact Pressure Results

(1)	(2)	(3)
Avg. TS IR	**P2 NOP**	**P2 SLB**
In	**Psi**	**psi** a,c,e

Table 2-6 Calculated Tubesheet Inner Diameter Dilation

Thermal Expansion of TS ID (in.)	[ ]a,c,e	
Tubesheet Elevation	**ΔP_{CREV} Expansion (in.)**	**Combined Expansion (in.)**
BTS		
NA		
TTS		

a,c,e

Table 2-7 Comparison of C^2 and Thick Shell Results

	Contact Pressure Results		
	TTS	NA	BTS
Max (psi)	[		
Min (psi)			
Average (psi)			
Thick Shell	[		

a,c,e

2.7 REFERENCES

2-1. WCAP-17072-P, "H*: Alternate Repair Criteria for the Tubesheet Expansion Region in Steam Generators with Hydraulically Expanded Tubes (Model D5)," May 2009.

2-2. *Stress Analysis of Thick Perforated Plates*, T. Slot, *Technomic Publishing Co., Westport, Conn.*, 1972.

2-3. LTR-SGDA-07-4 (Proprietary), "Letter Summary of Changes to B* and H* Analysis due to New Crevice Pressure and Divider Plate Data," Westinghouse Electric Company LLC, Pittsburgh, PA, January 17, 2007.

2-4. STD-MC-06-11-P, Rev. 1, "Pressure Profile Measurements during Tube-to-Tubesheet Leakage Tests of Hydraulically Expanded Steam Generator Tubing," Westinghouse Electric Company LLC, Pittsburgh, PA, August 30, 2007.

2-5. *Journal of Pressure Vessel Technology*, August 2006, Volume 128, Issue 3, pp. 408-413.

3 STRUCTURAL CALCULATIONS FOR H*

Section 2 of this report provided a description of the C^2 model, its intent, its design, how it fits in the overall process for calculating the H* distance and what its capabilities are relative to the model based on the thick shell equations. This section summarizes the actual analyses performed for the Model F and Model D5 SGs. Sections 3.1 through 3.3 summarize the significant assumptions in the application of the C^2 model, and the interface between the C^2 model and the 3-D FEA model of the lower tubesheet complex. Section 3.2 discusses the boundary conditions applied for the limiting Model D5 plant, Byron/Braidwood Unit 2, and the boundary conditions applied for the limiting Model F plant, Millstone Unit 3. Section 3.3 discusses the solution for the mean value of H*, including the displacement inputs from the 3-D FEA model and the axial contact pressure profiles each tubesheet radius for both the Model D5 and Model F SGs in both tabular and graphical form. Section 3.4 provides the probabilistic analysis based on the C^2 model for the Model D5 and Model F SGs. By its design and its interface with the 3-D FEA model of the lower tubesheet complex, the C^2 model cannot directly include the effect of Poisson contraction on H*; however, Section 3.5 provides the analysis of Poisson contraction on H* predicted using the C^2 model. In this section, Millstone Unit 3 and Byron/Braidwood Unit 2 are frequently discussed. Millstone Unit 3 is the limiting plant for the Model F SG plants and Byron/Braidwood Unit 2 are the identical limiting plants for the Model D5 SG plants. The criteria for defining the limiting plants are discussed in the current licensing basis (i.e., Reference 3-1 and 3-2). Section 3.6 discusses the inclusion of the crevice pressure adjustment to H* result. Section 3.7 provides a summary of the H* calculations and presents the final H* values.

3.1 OVERVIEW OF THE STRUCTURAL ANALYSIS FOR H*

As noted in Section 2 of this report, the C^2 model is a planar model of a tube in a tubesheet segment. The tubesheet segment can be visualized as a square local segment of the tubesheet that is defined by a single tube pitch ([ ]^{a,c,e} inches for the Model D5, [ ]^{a,c,e} inch for the Model F) centered on the location of a tube (see Figure 2-4). The model includes the tubesheet bore and a tube in its expanded diameter but without any residual contact pressure from the hydraulic expansion process. Thus, in its unloaded state, the tube is in zero-pressure line-on-line contact with the tubesheet bore.

The loading conditions applied to the square cell model are:

- Temperature, which varies axially through the tubesheet
- The internal tube pressure modified by the axially-dependent crevice pressure
- Planar displacements at the model boundaries, which are taken from the 3-D FEA model of the tubesheet complex when it is loaded by temperature increase and differential pressures applicable to the operating conditions of interest

In the licensing basis analysis, when applying the thick shell model, similar displacements were applied directly to the tubesheet bore; however, in the C^2 model application, the displacement conditions are applied to the boundaries of the model and the model determines the conditions at the actual tube-to-tubesheet interface. This is a key difference between the C^2 model and the thick shell model.

To calculate the axial contact pressure profile for a tube at the tubesheet radius of interest, the temperatures and displacements appropriate to the number of points considered through the thickness of the tubesheet are input separately to the model along with the tube wall pressure differential between the internal pressure of the tube, and the crevice pressure acting on the outer diameter of the tube wall and inner diameter of the tubesheet applicable to each elevation to determine the contact pressure between the tube and the tubesheet at each elevation. The elevations through the thickness of the tubesheet are consistent with the elevations utilized in the current licensing basis for H*. Application of the C^2 model assumes that the centerline of the tube remains straight, e.g., that no bending of the tubesheet occurs. The displacement input conditions, taken from the 3-D FEA model of the tubesheet complex, include the total effects of temperature and pressure loading in the continuum of the thickness of the tubesheet. Ignoring the coupling due to tubesheet bending in applying the C^2 model is a conservative application of this model because the introduction of tubesheet bore and tube bending would be expected to result in higher contact pressures between the tube and tubesheet.

The input boundary conditions include displacements in both axes of the plane. Conceptually, this is similar to the original analysis using the thick shell equations, but the application details are different. Previously, the radial displacement was taken directly from the 3-D FEA model, and the circumferential displacement was derived from the radial displacement (see Section 6.3 of WCAP-17072-P) and applied directly to the tubesheet bore. For application of the C^2 model, which is driven by the cell boundary displacements, it was desired that the radial displacements be calculated directly in the 3-D FEA model of the tubesheet complex. To facilitate this, the 3-D FEA model was modified by adding the same mesh used on the tubesheet centerline face perpendicular to the divider plate one and two pitches into the depth (not thickness) of the tubesheet. This permitted obtaining the displacements in the direction parallel to the divider plate directly from the 3-D FEA model for application to the C^2 model boundaries instead of direct application to the tubesheet bore.

The 3-D FEA model mesh was also modified for other reasons not directly related to application of the C^2 model. For example, to avoid applying a factor to account for a non-functional divider plate, the model was changed to directly reflect that the upper 5.0 inches of the divider plate were assumed to be non-existent (see Section 3.2.2 and Section 3.2.4). Further, changes were made to the 3-D FEA model mesh to properly represent the axial thermal profile through the thickness of the tubesheet (see Section 3.2.5).

3.2 STRUCTURAL ANALYSES (3-D FEA MODEL)

3.2.1 Method Discussion

The structural finite element analysis is based on a three-dimensional (3-D) model of the lower steam generator complex consisting of the channelhead, divider plate, tubesheet, and lower shell. The model uses Slot's effective material properties to model the perforated tubesheet section as an orthotropic material, as discussed in References 3-1 and 3-2. The plants are analyzed for low T_{avg} normal operating conditions (NOP) and steam line break (SLB), which have been determined to be limiting conditions in References 3-1, 3-2, and 3-18. Note that these conditions represent the bounding pressure and temperature values specified by the design basis transients and represent the design limits of the plant operating conditions but not the current actual plant operating conditions.

Because it was determined by consistent application of both the C^2 model and the thick shell model that the SLB condition is the limiting condition for H* for the Model D5 SGs, an analysis of the Model D5 SG was required using the 3-D FEA model to develop the SLB uncertainty surface to support the probabilistic H* analysis. This analysis is consistent with the methods documented in Reference 3-2. The results from the SLB 3-D FEA analysis for the Model D5 SGs, as documented in Reference 3-9, are utilized in Section 3.4 for the Model D5 probabilistic analysis.

3.2.2 Assumptions

The assumptions below, with the exception of the thermal temperature profile through the tubesheet, are copied from References 3-1 and 3-2. For each analysis condition, a thermal and a combined thermal-structural analysis were performed to determine the deformations in the tubesheet. All of the finite element analysis (FEA) results assume a static, steady-state, linear, and elastic system.

An analysis performed in Reference 3-3 concludes that, in general, the tubesheet is approximately at the primary side temperature through its thickness, except for a sharp thermal gradient that exists in approximately the top one (1.00) inch. In the thermal analysis, the secondary side of the tubesheet was assumed to be at a temperature equal to the average of the steam temperature and the feedwater temperature. The tubesheet portion of the 3-D FEA model used in this analysis was partitioned two inches from the top of the tubesheet. From the bottom of the tubesheet to the top of this partition in the tubesheet, an approximately uniform temperature equal to the hot leg temperature was applied. This produced a temperature gradient in the top two inches of the tubesheet from a value of 10 degrees cooler than the primary fluid temperature to the average of the coldest allowable condition-specific feedwater and steam outlet temperatures as specified by the applicable Performance Capability Working Group (PCWG). See Section 5 of References 3-1, 3-2, and the letter noted as Reference 3-18, for details. For the SLB case, the primary fluid and the average of the secondary fluids (steam and feedwater) were applied to the primary and secondary surfaces of the tubesheet, respectively, so that a linear temperature gradient developed through the thickness of the tubesheet. This is a reasonable assumption because the long-term portion of the transient specifies that flow will be reduced to natural circulation through the affected loop when the reactor coolant pumps are off.

Where a range of feedwater temperatures was specified in the PCWG parameters, the condition most conservative for H* was used. Since H* values are negatively impacted (i.e., greater H* values result) by large radial deformations of the tubesheet, a higher overall temperature of the tubesheet will result in a lower modulus, and thus a conservative H* value. Therefore the higher feedwater temperature was used.

The structural analyses for the SLB transient are performed statically. The analysis inputs for the SLB condition include the maximum pressure differential over the entire transient definition and the asymptotic temperature reached long after the initiation of the event. In the component hardware design transient, even though the plant is initially at no-load conditions, it is assumed that the steam line break results in an immediate reactor trip and actuation of the safety injection system. The transient also assumes that off-site power is lost at the time of the break and all reactor coolant pumps are de-energized so that coolant flow coasts down to the natural circulation value. The maximum pressure differential occurs because the safety injection system operates at design capacity and re-pressurizes the system in a relatively short time. It is conservative to use the stated conditions because the more realistic scenario would be that a reduction in pressure would occur across the tubes and tubesheet over the long-term

duration of the event due to operator actions consistent with the plant Emergency Operator Procedures (EOPs). The EOPs, for an event which includes safety injection, provide for reduction/termination of safety injection flow and for the initiation of cool-down and depressurization of the reactor coolant system to the point that the residual heat removal system can be placed in operation for continued cooling of the RCS.

The finite element model did not include the nozzles or manways. This is reasonable because the deformations of interest are in the tubesheet, which is well removed from the channelhead penetrations, and thus, would not be expected to have a significant effect on tubesheet deflections. Prior analysis has shown that including the larger channelhead penetrations, such as the manways, tends to decrease displacements in the tubesheet. Decreasing tubesheet displacements will produce shorter H* distances; therefore, the current approach is conservative. The model did not consider the tubes or any of the structure above the tubesheet except the lower shell (stub barrel). Including the portion of the tube within the tubesheet decreases the tubesheet displacement because it stiffens the tubesheet with respect to the bending caused by the primary-to-secondary pressure differential (Reference 3-7).

References 3-1 and 3-2 show that it is conservative to neglect the structural support that the divider plate provides to the tubesheet. Therefore, in the 3-D finite element model of the Model F SG and the Model D5 SG, the divider plate is severed from the tubesheet and provides no direct structural support to the tubesheet in this analysis. This is discussed in Section 3.2.4. Consistent with previous applications, it is noted that the Model F SG and the Model D5 SGs considered in the structural analysis are model specific, e.g., the dimensions of the divider plate, channel head and lower shell are specific to the model of SG considered.

3.2.3 Input

The input for this analysis consists of steam generator dimensions for the plants to be analyzed, material properties from the ASME Code, and pressure and temperature conditions from the PCWG parameters and transients.

The input boundary conditions for the limiting plants are Table 3-1 and Table 3-2 for the Model F plants and Model D5 plants, respectively. The modulus of elasticity and coefficients of thermal expansion are provided in Table 3-3 and Table 3-4. The tubesheet is SA-508 Class 2A, the divider plate is Alloy 600 (SB-168), the channelhead is SA-216 Grade WCC, and the lower shell is SA-533 Grade A Class 2. These are the same values included in References 3-1 and 3-2.

3.2.4 Geometry

The structural model geometry analyzed for the Model F and D5 SGs is essentially identical to that considered in the baseline analyses in References 3-1 and 3-2. The only modifications were the addition of several model partitions in the tubesheet region and truncating the divider plate. The first partition in the tubesheet model is at two inches from the secondary surface to accommodate a non-linear temperature profile. Additional solid body partitions were made through the tubesheet at distances equal to one and two pitches behind the half-symmetry plane to facilitate the post-processing of displacements for the square cell model. The typical solid models used are shown in Figure 3-1 for the Model F SGs

(Millstone Unit 3) showing the truncated divider plate and Figure 3-2 for the Model D5 SG (Byron/Braidwood Unit 2) showing the model with the intact divider plate.

In References 3-1 and 3-2, concerns regarding the potential for divider plate cracking were addressed by applying a "divider plate factor" to represent whether, or not, the divider plate provides structural support. This condition is discussed in Reference 3-4, which details the assessment of a fully degraded divider plate-to-tubesheet weld in terms of the divider plate factors discussed in Reference 3-1, Section 6.2.6. In the current analysis, the 3-D FEA lower tubesheet complex model was modified to exclude the upper five inches of the divider plate to decouple it from the tubesheet; however, the divider plate was still included in the channelhead. This structural model variant eliminated the need to apply the divider plate factor because the structural model directly addresses the presumed degraded divider plate. Application of this model confirmed the conclusions of Reference 3-1 that this assumption is conservative relative to H*.

Figure 3-1 shows a representation of the solid body with the upper five inches of the divider plate and attached materials suppressed. Eliminating this material in the model does not change the application or values of the applied boundary conditions nor does it change the results of the thermal analysis. The only effect that truncating the divider plate has is that the tubesheet has less resistance to the applied pressure loads than if it were connected to the divider plate. However, in all other respects, the steam generator model with the severed divider plate is the same model as the steam generator with an intact divider plate.

3.2.5 Mesh Discussion

The model meshes for all models of SGs among the H* candidate population are similar but are adjusted to accommodate the specific geometry of each model of SG. The model meshes used in the analyses for the Models F and D5 SGs are essentially the same as the meshes documented in References 3-1 and 3-2. Additional constraints were added to the current mesh to accommodate the vertical partition through the tubesheet. The typical mesh used is shown in Figure 3-3, Figure 3-4, and Figure 3-5 for the principal axes. Although the Model F mesh is shown, the mesh for the Model D5 is similar to that shown in Figure 3-3, Figure 3-4 and Figure 3-5.

3.2.6 Tubesheet Equivalent Properties

Modeling of the equivalent properties of the perforated plate (tubesheet) by the method of Slot is discussed in Section 6.2.1 of References 3-1 and 3-2. The same equivalent properties used in References 3-1 and 3-2 were used in the current analysis. Information from those references is included here for completeness. Interpolated ratios of equivalent properties are in Table 3-5, where the "*" indicates the properties of the equivalent tubesheet. The ratios are then multiplied by the material properties for SA-508 Class 2A in Table 3-3 to obtain the temperature-dependent equivalent properties. The equivalent properties for the tubesheet are in Table 3-6 and Table 3-7 for the Model F SG and Model D5 SG, respectively.

3.2.7 Boundary Conditions

The application of the boundary conditions to the models is consistent with those included in the current licensing basis, Reference 3-1 and Reference 3-2. Table 3-1 and Table 3-2 summarize the specific boundary conditions and how they are applied to the 3-D FEA model. Two different analyses were performed with the 3-D FEA model of the lower SG tubesheet complex to support application of the C^2 model:

1. Thermal Analysis: The absolute operating temperature conditions were applied to the SG, as opposed to a difference in temperature with a reference temperature of 70°F. The result from this analysis is purely a temperature profile through the tubesheet.

2. Deflection Analysis: In this analysis, the non-uniform temperature profile from the first analysis and the pressure loads are simultaneously applied to the model. The results from this analysis, with the severed divider plate condition, are used in the final H* analysis, instead of accounting for the absence of the divider plate by application of a divider plate factor, as in the licensing basis analysis. All of the required displacements and effects are directly accounted for by *ANSYS*.

The results of the second analysis provide the input for subsequent analysis with the square cell model which replaces the thick shell model in the current licensing basis. The approach in the deflection analysis is beneficial because it eliminates the need to separately post-process and calculate the different displacements required for the H* analysis, as was done in the licensing basis.

The applied loads and temperatures in each analysis are shown in Table 3-1 and Table 3-2. The analysis was applied only to the limiting conditions required for H*; that is, if a plant's limiting H* distance is controlled by the normal operating (NOP) condition, the NOP pressures and temperature loads were used in the analysis and the SLB conditions were not considered and vice versa (see Section 3.3.11 for the limiting operating conditions for the Model F and Model D5 SGs).

3.2.8 Tubesheet Complex 3-D FEA Analysis Results

Typical results of the thermal analysis for Millstone for normal operating conditions are shown in Figure 3-6. The thermal profile shown in Figure 3-6 is more accurate than that shown in Reference 3-1 (and, as appropriate, in Reference 3-2) due to the direct application of temperature loads to the tubesheet partition. Figure 3-7 through Figure 3-9 show the results of the thermal-structural analysis for Millstone Unit 3 for 100% power. Figure 3-10 shows the results of the SLB thermal analysis for Millstone Unit 3. Figure 3-11 and Figure 3-12 show the X- and Z-deformations for SLB for Millstone Unit 3. The results of the current 3-D FEA are taken from Reference 3-6.

Table 3-1 Input Boundary Conditions for Model F (Millstone Unit 3)

Parameter	Low T_{avg}	SLB
Hot Leg Pressure (psia)		
SG Outlet Pressure (psia)		
Secondary Pressure (psia)		
Hot Leg Temperature (°F)		
SG Outlet Temperature (°F)		
Steam Temperature (°F)		
Feedwater Temperature (°F)		
Mean Shell Radius r_m (inches)		
Shell Thickness t (inches)		
Calculated Values		
Secondary Fluid Temperature		
End Cap Load (psia)		

a,c,e

a,c,e

Table 3-2 Input Boundary Conditions for Model D5 (Byron/Braidwood Unit 2)

Parameter	Low T_{avg}	SLB
Hot Leg Pressure (psia)		
SG Outlet Pressure (psia)		
Secondary Pressure (psia)		
Hot Leg Temperature (°F)		
SG Outlet Temperature (°F)		
Steam Temperature (°F)		
Feedwater Temperature (°F)		
Mean Shell Radius r_m (inches)		
Shell Thickness t (inches)		
Calculated Values		
Secondary Fluid Temperature		
End Cap Load (psia)		

a,c,e

a,c,e

Table 3-3 Modulus of Elasticity for Materials

Temperature (°F)	SA-508 Class 2A (Msi)	Alloy 600 (Msi)	SA-216 Grade WCC (Msi)	SA-533 Grade A Class 2 (Msi)
70	29.2	31.0	29.5	29.2
200	28.5	30.2	28.8	28.5
300	28.0	29.9	28.3	28.0
400	27.4	29.5	27.7	27.4
500	27.0	29.0	27.3	27.0
600	26.4	28.7	26.7	26.4
700	25.3	28.2	25.5	25.3

Table 3-4 Coefficient of Thermal Expansion for Materials

Temperature (°F)	SA-508 Class 2A (µin/in)	Alloy 600 (µin/in)	SA-216 Grade WCC (µin/in)	SA-533 Grade A Class 2 (µin/in)
70	6.50	6.90	5.53	7.06
200	6.67	7.20	5.89	7.25
300	6.87	7.40	6.26	7.43
400	7.07	7.57	6.61	7.58
500	7.25	7.70	6.91	7.70
600	7.42	7.82	7.17	7.83
700	7.59	7.94	7.41	7.94

Table 3-5 Interpolated Ratios of Equivalent Material Properties for Analysis of Perforated Plate

Property	Model F[1]	Model D5
Gy*/Gy	[	
Ey*/Ey		
Ep*/Ep		
Gp*/Gp		
Poisson's Ratio	[	

a,c,e

Notes:
1. These values differ from the values shown in Reference 3-1; however, they are the actual values used in the analysis documented in Reference 3-1.

Table 3-6 Equivalent Properties for Tubesheet for Model F SG (Millstone Unit 3)

Temperature (°F)	Out-of-Plane		In-Plane		a,c,e
	E (Msi)	G (Msi)	E (Msi)	G (Msi)	
70					
200					
300					
400					
500					
600					
700					

Table 3-7 Equivalent Properties for Tubesheet for Model D5 SG (Byron/Braidwood Unit 2)

Temperature (°F)	Out-of-Plane		In-Plane		a,c,e
	E (Msi)	G (Msi)	E (Msi)	G (Msi)	
70					
200					
300					
400					
500					
600					
700					

a,c,e

Figure 3-1 Typical Representation of Severed Divider Plate Condition; Model F (Millstone Unit 3 configuration shown)

a,c,e

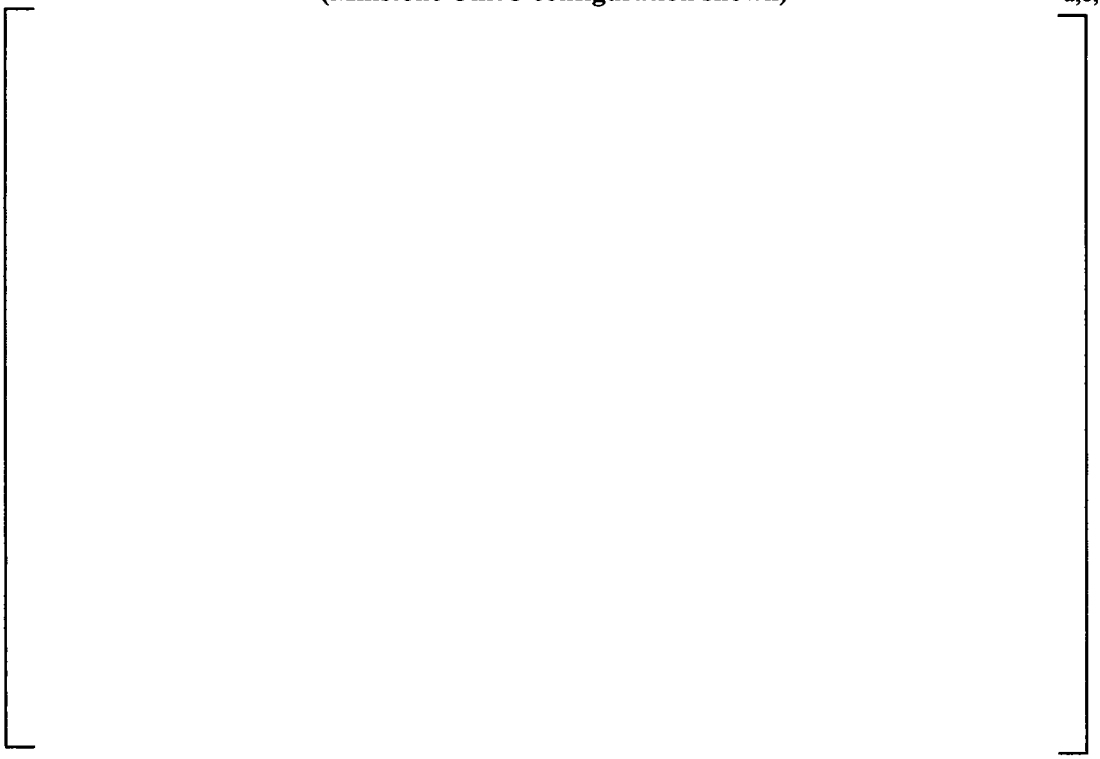

Figure 3-2 Typical Solid Model for Intact Divider Plate; Model D5 (Byron/Braidwood Unit 2 configuration shown)

a,c,e

Figure 3-3 Model F (Millstone Unit 3) Mesh, View Down Z-Axis

a,c,e

Figure 3-4 Model F (Millstone Unit 3) Mesh, View Down Y-Axis

a,c,e

Figure 3-5 Model F (Millstone Unit 3) Mesh, View Down X-Axis

a,c,e

Figure 3-6 Model F (Millstone Unit 3) Results of NOP Thermal Analysis

a,c,e

Figure 3-7 Model F (Millstone Unit 3) Results of Thermal-Structural Analysis, Y Deformation

a,c,e

Figure 3-8 Model F (Millstone Unit 3) Results of Thermal-Structural Analysis, X Deformation on Hot Leg Face

a,c,e

Figure 3-9 Model F (Millstone Unit 3) Results of Thermal-Structural Analysis, Z Deformation on Hot Leg

a,c,e

Figure 3-10 Model F (Millstone Unit 3) Results of SLB Thermal Analysis

a,c,e

Figure 3-11 Model F (Millstone Unit 3) Results of SLB Thermal-Structural Analysis, X Deformation on Hot Leg Face

a,c,e

Figure 3-12 Model F (Millstone Unit 3) Results of SLB Thermal-Structural Analysis, Z Deformation on Hot Leg

3.3 CALCULATION OF MEAN H* FROM C^2 MODEL

3.3.1 Method Discussion

The structural analysis for the tube-to-tubesheet contact pressures is based on a 2-D finite element model. The 2-D finite element model is a pseudo sub-model of the SG tubesheet and corresponding tube in increments throughout the entire tubesheet thickness of approximately 21 inches. This model is then quartered to simplify the computations as seen in Figure 3-13.

Each tubesheet radius of each SG model is computed and graphed separately. At each tubesheet radius, there are twelve and thirteen elevations, respectively, for the Model F and D5 SGs at which the contact pressure is calculated. (An exception is for the Model D5 FLB condition for which only nine elevations are calculated.) For each operating condition, a thermal and thermal-structural analysis was performed with the 3-D FEA model (see Sections 3.1 and 3.2) to determine the tubesheet displacements used as input to the square cell model to calculate the contact pressures of the tubes with regards to the tubesheet. All of the analyses were static and linear elastic.

a,c,e

Figure 3-13 Sub-Model for Computational Analysis

3.3.2 Development of Displacements for Square Cell

The displacements to apply to the square cell model are calculated from the displacements on the 3-D model using a finite difference technique to approximate the strain. The applied displacements simulate the strain across one-half of one pitch of the steam generator from all of the loads applied to the 3-D FEA model. There are two displacements to consider, those in the X-direction and those in the

Z-direction (both in the same plane). For calculation of the displacements in the X-direction, the X-displacements on the hot leg face of the perforated section of the tubesheet are utilized. After being exported from *ANSYS*, they are processed using a finite difference method to calculate the strain, which is the derivative of displacement. This utilizes the central difference formula of second order (Reference 3-5, pp 83-85):

$$\varepsilon_i = \frac{\partial U_{x,i}}{\partial x} \approx \frac{U_{x,i+1} - U_{x,i-1}}{2\Delta x} \qquad \text{(Equation 3-1)}$$

At the edges of the perforated region, of necessity, the forward and backward differences of second order are used:

$$\varepsilon_i = \frac{\partial U_{x,i}}{\partial x} \approx \frac{-U_{x,i+2} + 4U_{x,i+1} - 3U_{x,i}}{2\Delta x}$$
$$\varepsilon_i = \frac{\partial U_{x,i}}{\partial x} \approx \frac{+U_{x,i-2} - 4U_{x,i-1} + 3U_{x,i}}{2\Delta x} \qquad \text{(Equation 3-2)}$$

The displacement to apply to the square cell model is the strain times the length of the model, which is one-half of a pitch:

$$\Delta x_{squarecell} = 0.5 * P * \varepsilon_x \qquad \text{(Equation 3-3)}$$

The calculation of the z-displacements uses the z-displacements from the 3-D FEA model which are two pitches back from the hot leg face. A similar central difference formula is used to calculate the derivative:

$$\varepsilon_i = \frac{\partial U_{z,i}}{\partial z} \approx \frac{U_{z,i+2} - U_{z,i}}{2\Delta z} \qquad \text{(Equation 3-4)}$$

This equation is slightly modified to calculate the strain in the z-direction one pitch back from the cut face of the 3-D model. This is necessary because the cut face has a symmetry condition in the z-direction; therefore, the strain in the z-direction necessarily vanishes there. Since the displacement is zero on that face, the equation can be simplified:

$$\varepsilon_i = \frac{\partial U_{z,i}}{\partial z} \approx \frac{U_{z,i+2}}{2P} \qquad \text{(Equation 3-5)}$$

Calculation of the applied displacements from the strain is identical:

$$\Delta z_{squarecell} = 0.5 * P * \varepsilon_z \qquad \text{(Equation 3-6)}$$

3.3.3 Assumptions

The axial thermal profile for the tubesheet is discussed in Section 3.2. In the thermal analysis, the secondary side of the tubesheet was assumed to be at a temperature equal to the average of the steam temperature and the feedwater temperature.

For the connections between the tube and tubesheet, this model uses a friction coefficient of [ ]^{a,c,e} (References 3-1 and 3-2), and a pinball radius of [ ]^{a,c,e} inches, which is half the value of the surface roughness tolerance from Reference 3-13. The analysis also uses a normal stiffness factor of [ ]^{a,c,e}, which determines how quickly the model will converge depending on the degree of bending deformation, which was based on several trials that defined this value for acceptable convergence of the model.

The square cell model does not use the Goodier model, and does not assume the tubesheet collar is a continuous structure. The applied loading on the tubesheet bends the tube within the tubesheet because the tube is a continuous structure. This bending is caused by temperature change as well as the pressure differential across the tubesheet and increases contact pressure. Neglecting tubesheet bending is conservative because the increased contact pressure between the tube and the tubesheet would reduce the H* distance.

3.3.4 Input

The input for this analysis consists of steam generator dimensions for the limiting Model F and Model D5 plants, material properties from the ASME Code, and pressure and temperature conditions from the PCWG parameters and transients. The dimensions, the material properties, and the PCWG parameters used for the D5 and F models are taken from References 3-1, 3-2, and 3-18, respectively.

Because the analysis is a static, linear, elastic methodology, the material properties used as inputs are the elastic moduli and coefficients of thermal expansion. The tubesheet is SA-508 Class 2A and the tube is Alloy 600 Thermally Treated (TT). The modulus of elasticity and coefficients of thermal expansion are taken from References 3-1 and 3-2.

3.3.5 Geometry

Figure 3-14 shows a representation of the solid model used. The model was created in *ANSYS* Workbench Design Modeler. The associated representative dimensions for all models are shown in Figure 3-15.

3.3.6 Mesh

The mesh used in the analysis combines the tube and tubesheet in one model and creates one mesh for both pieces. This grid of nodes allows for easy post-processing and interpolation of deformations on the face. The density in this region is judged to be adequate from experience and comparison to prior models (i.e., Reference 3-6). The actual mesh for all models analyzed is shown in Figure 3-16.

a,c,e

Figure 3-14 Representative Solid Model

a,c,e

Figure 3-15 Representative Dimensions for All Models

a,c,e

Figure 3-16 Implemented Model Mesh, View Down Z-Axis

3.3.7 Boundary Conditions

The applied boundary conditions consisted of pressure loads, thermal loads, and constraints. The pressure loads consist of the internal fluid pressure and the crevice pressure, which is represented as the pressure difference on the inside surface of the tube. The thermal loads were applied as fixed temperature boundary conditions on the bodies for the thermal analysis. Three constraints applied.

1. The upper edge of the model was constrained in the X-direction.

2. The lower edge of the model was constrained in the Y-direction.

3. The pressure differential on the tube was determined as the difference between the primary pressure on the tube ID and the crevice pressure on the tube OD.

The application of these boundary conditions is shown in Figure 3-17.

All of the applied loads and temperatures are described in Section 3.2.

(Note: For analytical convenience, the coordinate system for this model is X-Y, which is equivalent to the X-Z SG coordinates as noted in Section 2.)

a,c,e

Figure 3-17 Boundary Conditions for All Models

3.3.8 C^2 FEA Results

Inputs and contact pressure plots of the finite element analysis (FEA) results for each individual model, radius and elevation are included in this section. The thermal analysis results are steady-state with fixed boundary conditions (Reference 3-8).

Within each table, the explanations of the categories are as follows: TS Elevation stands for tubesheet elevation, ΔX and ΔZ represent the displacement in the respective direction of the square cell model, ΔP represents the difference between the reference pressure and the crevice pressure which was empirically determined, the temperature of the tubesheet, and "P_{con} Theta" represents the contact pressure between the tube and tubesheet.

3.3.9 Model D5 (Byron/Braidwood Unit 2) Square Cell Model Results

Contact pressure axial profiles were calculated at the same six radii considered in Reference 3-2 to provide directly comparable results between the C^2 model and the thick shell equation model used in Reference 3-2. The results based on the C^2 model calculations for the Model D5 are provided in Table 3-8 through Table 3-13. Tables are provided for each of the NOP, SLB, and FLB conditions in this section; the FLB condition figures appear in Section 4 to support the leakage assessment. In these tables, the zero reference is the top of the tubesheet.

The tabular results in Table 3-8 through Table 3-13 are shown graphically in Figure 3-18 through Figure 3-23. These figures show the contact pressure trends of the normal operating condition compared to the steam line break conditions at various elevations between 0.0 and 21.03 inches, where 0.0 represents the top of the tubesheet and 21.03 represents the bottom of the tubesheet.

3.3.10 Model F (Millstone Unit 3) Square Cell Model Results

Contact pressure axial profiles were calculated at the same six radii considered in Reference 3-1 to provide directly comparable results between the C^2 model and the thick shell equation model used in Reference 3-1.The results based on the C^2 model calculations for the Model F SGs are provided in Table 3-14 through Table 3-19. Tables are provided for the NOP and SLB conditions.

The tabular results in Table 3-14 through Table 3-19 are shown graphically in Figure 3-24 through Figure 3-29. These figures show the contact pressure trends of the normal operating condition compared to the steam line break conditions at various elevations between 0.0 and 21.03 inches, where 0.0 represents the top of the tubesheet and 21.03 represents the bottom of the tubesheet.

The selection of zero reference in the tables and figures is the same as for the Model D5 discussed in Section 3.3.9.

A qualitative assessment of the factors that influence contact pressure was performed (Reference 3-14) which shows that contact pressures for FLB conditions would exceed those in the current licensing basis, and thus, explicit analysis is unnecessary.

Table 3-8 Model D5 Byron/Braidwood Unit 2 Inputs and Results, 4.437 in. Radius

NOP							
	TS Elevation	ΔX	ΔZ	ΔP	Temperature	P_{CON} Theta	a,c,e
	in	in	in	psi	°F	psi	
BTS	21.03						
	19.03						
	17.03						
	15.03						
	12.77						
NA	10.52						
	8.53						
	6.03						
	4.13						
	3.03						
	2.00						
	1.00						
TTS	0.00						
SLB							
	TS Elevation	ΔX	ΔZ	ΔP	Temperature	P_{CON} Theta	a.c.e
	in	n	in	psi	°F	psi	
BTS	21.03						
	19.03						
	17.03						
	15.03						
	12.77						
NA	10.52						
	8.53						
	6.03						
	4.13						
	3.03						
	2.00						
	1.00						
TTS	0.00						
FLB							
	TS Elevation	ΔX	ΔZ	ΔP	Temperature	P_{CON} Theta	a,c,e
	in	in	in	psi	°F	psi	
BTS	21.03						
	19.03						
	17.03						
	15.03						
NA	10.52						
	4.13						
	2.00						
	1.00						
TTS	0.00						

Table 3-9 Model D5 Byron/Braidwood Unit 2 Inputs and Results, 10.431 in. Radius

NOP							
	TS Elevation	ΔX	ΔZ	ΔP	Temperature	P_{CON} Theta	
	in	in	in	psi	°F	psi	a,c,e
BTS	21.03	[					
	19.03						
	17.03						
	15.03						
	12.77						
NA	10.52						
	8.53						
	6.03						
	4.13						
	3.03						
	2.00						
	1.00						
TTS	0.00	]					]
SLB							
	TS Elevation	ΔX	ΔZ	ΔP	Temperature	P_{CON} Theta	
	in	in	in	psi	°F	psi	a,c,e
BTS	21.03	[					
	19.03						
	17.03						
	15.03						
	12.77						
NA	10.52						
	8.53						
	6.03						
	4.13						
	3.03						
	2.00						
	1.00						
TTS	0.00	]					]
FLB							
	TS Elevation	ΔX	ΔZ	ΔP	Temperature	P_{CON} Theta	
	in	in	in	psi	°F	psi	a,c,e
BTS	21.03	[					
	19.03						
	17.03						
	15.03						
NA	10.52						
	4.13						
	2.00						
	1.00						
TTS	0.00	]					]

Table 3-10 Model D5 Byron/Braidwood Unit 2 Inputs and Results, 18.139 in. Radius

NOP							
	TS Elevation	ΔX	ΔZ	ΔP	Temperature	P_{CON} Theta	a,c,e
	in	in	in	psi	°F	psi	
BTS	21.03						
	19.03						
	17.03						
	15.03						
	12.77						
NA	10.52						
	8.53						
	6.03						
	4.13						
	3.03						
	2.00						
	1.00						
TTS	0.00						
SLB							
	TS Elevation	ΔX	ΔZ	ΔP	Temperature	P_{CON} Theta	a,c,e
	in	in	in	psi	°F	psi	
BTS	21.03						
	19.03						
	17.03						
	15.03						
	12.77						
NA	10.52						
	8.53						
	6.03						
	4.13						
	3.03						
	2.00						
	1.00						
TTS	0.00						
FLB							
	TS Elevation	ΔX	ΔZ	ΔP	Temperature	P_{CON} Theta	a,c,e
	in	in	in	psi	°F	psi	
BTS	21.03						
	19.03						
	17.03						
	15.03						
NA	10.52						
	4.13						
	2.00						
	1.00						
TTS	0.00						

Table 3-11 Model D5 Byron/Braidwood Unit 2 Inputs and Results, 26.703 in. Radius

NOP							
	TS Elevation	ΔX	ΔZ	ΔP	Temperature	P_{CON} Theta	
	in	in	in	psi	°F	psi	a,c,e
BTS	21.03	[					
	19.03						
	17.03						
	15.03						
	12.77						
NA	10.52						
	8.53						
	6.03						
	4.13						
	3.03						
	2.00						
	1.00						
TTS	0.00						
SLB							
	TS Elevation	ΔX	ΔZ	ΔP	Temperature	P_{CON} Theta	
	in	in	in	psi	°F	psi	a,c,e
BTS	21.03	[					
	19.03						
	17.03						
	15.03						
	12.77						
NA	10.52						
	8.53						
	6.03						
	4.13						
	3.03						
	2.00						
	1.00						
TTS	0.00						
FLB							
	TS Elevation	ΔX	ΔZ	ΔP	Temperature	P_{CON} Theta	
	in	in	in	psi	°F	psi	a,c,e
BTS	21.03	[					
	19.03						
	17.03						
	15.03						
NA	10.52						
	4.13						
	2.00						
	1.00						
TTS	0.00						

Table 3-12 Model D5 Byron/Braidwood Unit 2 Inputs and Results, 42.974 in. Radius

NOP							
	TS Elevation	ΔX	ΔZ	ΔP	Temperature	P_{CON} Theta	
	in	in	in	psi	°F	psi	a,c,e
BTS	21.03	[					
	19.03						
	17.03						
	15.03						
	12.77						
NA	10.52						
	8.53						
	6.03						
	4.13						
	3.03						
	2.00						
	1.00						
TTS	0.00	]					]
SLB							
	TS Elevation	ΔX	ΔZ	ΔP	Temperature	P_{CON} Theta	
	in	in	in	psi	°F	psi	a,c,e
BTS	21.03	[					
	19.03						
	17.03						
	15.03						
	12.77						
NA	10.52						
	8.53						
	6.03						
	4.13						
	3.03						
	2.00						
	1.00						
TTS	0.00	]					]
FLB							
	TS Elevation	ΔX	ΔZ	ΔP	Temperature	Pcon Theta	
	in	in	in	psi	°F	psi	a,c,e
BTS	21.03	[					
	19.03						
	17.03						
	15.03						
NA	10.52						
	4.13						
	2.00						
	1.00						
TTS	0.00	]					]

Table 3-13 Model D5 Byron/Braidwood Unit 2 Inputs and Results, 49.825 in. Radius

NOP							
	TS Elevation	ΔX	ΔZ	ΔP	Temperature	P_{CON} Theta	
	in	in	in	psi	°F	psi	a,c,e
BTS	21.03						
	19.03						
	17.03						
	15.03						
	12.77						
NA	10.52						
	8.53						
	6.03						
	4.13						
	3.03						
	2.00						
	1.00						
TTS	0.00						
SLB							
	TS Elevation	ΔX	ΔZ	ΔP	Temperature	P_{CON} Theta	
	in	in	in	psi	°F	psi	a,c,e
BTS	21.03						
	19.03						
	17.03						
	15.03						
	12.77						
NA	10.52						
	8.53						
	6.03						
	4.13						
	3.03						
	2.00						
	1.00						
TTS	0.00						
FLB							
	TS Elevation	ΔX	ΔZ	ΔP	Temperature	P_{CON} Theta	
	in	in	in	psi	°F	psi	a,c,e
BTS	21.03						
	19.03						
	17.03						
	15.03						
NA	10.52						
	4.13						
	2.00						
	1.00						
TTS	0.00						

Table 3-14 Model F Millstone Unit 3 Inputs and Results, 4.016 in. Radius

NOP							
	TS Elevation	ΔX	ΔZ	ΔP	Temperature	P_{CON} Theta	a,c,e
	in	in	in	psi	°F	psi	
BTS	21.03						
	19.03						
	17.03						
	15.03						
	13.03						
NA	10.52						
	8.53						
	6.03						
	4.13						
	2.00						
	1.00						
TTS	0.00						

SLB							
	TS Elevation	ΔX	ΔZ	ΔP	Temperature	P_{CON} Theta	a,c,e
	in	in	in	psi	°F	psi	
BTS	21.03						
	19.03						
	17.03						
	15.03						
	13.03						
NA	10.52						
	8.53						
	6.03						
	4.13						
	2.00						
	1.00						
TTS	0.00						

Table 3-15 Model F Millstone Unit 3 Inputs and Results, 11.722 in. Radius

NOP							
	TS Elevation	**ΔX**	**ΔZ**	**ΔP**	**Temperature**	**P_{CON} Theta**	
	in	**in**	**in**	**psi**	**°F**	**psi**	a,c,e
BTS	21.03	[					
	19.03						
	17.03						
	15.03						
	13.03						
NA	10.52						
	8.53						
	6.03						
	4.13						
	2.00						
	1.00						
TTS	0.00	]					

SLB							
	TS Elevation	**ΔX**	**ΔZ**	**ΔP**	**Temperature**	**P_{CON} Theta**	
	in	**in**	**in**	**psi**	**°F**	**psi**	a,c,e
BTS	21.03	[					
	19.03						
	17.03						
	15.03						
	13.03						
NA	10.52						
	8.53						
	6.03						
	4.13						
	2.00						
	1.00						
TTS	0.00	]					

Table 3-16 Model F Millstone Unit 3 Inputs and Results, 20.498 in. Radius

NOP						
	TS Elevation	**ΔX**	**ΔZ**	**ΔP**	**Temperature**	**P_{CON} Theta**
	in	**in**	**in**	**psi**	**°F**	**psi**
BTS	21.03	[				
	19.03					
	17.03					
	15.03					
	13.03					
NA	10.52					
	8.53					
	6.03					
	4.13					
	2.00					
	1.00					
TTS	0.00	]				

a,c,e

SLB						
	TS Elevation	**ΔX**	**ΔZ**	**ΔP**	**Temperature**	**P_{CON} Theta**
	in	**in**	**in**	**psi**	**°F**	**psi**
BTS	21.03	[				
	19.03					
	17.03					
	15.03					
	13.03					
NA	10.52					
	8.53					
	6.03					
	4.13					
	2.00					
	1.00					
TTS	0.00	]				

a,c,e

Table 3-17 Model F Millstone Unit 3 Inputs and Results, 30.193 in. Radius

NOP						
	TS Elevation	**ΔX**	**ΔZ**	**ΔP**	**Temperature**	**P_{CON} Theta**
	in	**in**	**in**	**psi**	**°F**	**psi**
BTS	21.03					
	19.03					
	17.03					
	15.03					
	13.03					
NA	10.52					
	8.53					
	6.03					
	4.13					
	2.00					
	1.00					
TTS	0.00					

a,c,e

SLB						
	TS Elevation	**ΔX**	**ΔZ**	**ΔP**	**Temperature**	**P_{CON} Theta**
	in	**in**	**in**	**psi**	**°F**	**psi**
BTS	21.03					
	19.03					
	17.03					
	15.03					
	13.03					
NA	10.52					
	8.53					
	6.03					
	4.13					
	2.00					
	1.00					
TTS	0.00					

a,c,e

Table 3-18 Model F Millstone Unit 3 Inputs and Results, 48.613 in. Radius

NOP						
	TS Elevation	**ΔX**	**ΔZ**	**ΔP**	**Temperature**	**P_{CON} Theta**
	in	**in**	**in**	**psi**	**°F**	**psi**
BTS	21.03					
	19.03					
	17.03					
	15.03					
	13.03					
NA	10.52					
	8.53					
	6.03					
	4.13					
	2.00					
	1.00					
TTS	0.00					

a,c,e

SLB						
	TS Elevation	**ΔX**	**ΔZ**	**ΔP**	**Temperature**	**P_{CON} Theta**
	in	**in**	**in**	**psi**	**°F**	**psi**
BTS	21.03					
	19.03					
	17.03					
	15.03					
	13.03					
NA	10.52					
	8.53					
	6.03					
	4.13					
	2.00					
	1.00					
TTS	0.00					

a,c,e

Table 3-19 Model F Millstone Unit 3 Inputs and Results, 58.308 in. Radius

NOP							
	TS Elevation	ΔX	ΔZ	ΔP	Temperature	P_{CON} Theta	
	in	in	in	psi	°F	psi	a,c,e
BTS	21.03	[					
	19.03						
	17.03						
	15.03						
	13.03						
NA	10.52						
	8.53						
	6.03						
	4.13						
	2.00						
	1.00						
TTS	0.00	]					

SLB							
	TS Elevation	ΔX	ΔZ	ΔP	Temperature	P_{CON} Theta	
	in	in	in	psi	°F	psi	a,c,e
BTS	21.03	[					
	19.03						
	17.03						
	15.03						
	13.03						
NA	10.52						
	8.53						
	6.03						
	4.13						
	2.00						
	1.00						
TTS	0.00	]					

a,c,e

Figure 3-18 Model D5 Contact Pressure Results, 4.437 in. Radius

a,c,e

Figure 3-19 Model D5 Contact Pressure Results, 10.431 in. Radius

a,c,e

Figure 3-20 Model D5 Contact Pressure Results, 18.139 in. Radius

a,c,e

Figure 3-21 Model D5 Contact Pressure Results, 26.703 in. Radius

a,c,e

Figure 3-22 Model D5 Contact Pressure Results, 42.974 in. Radius

a,c,e

Figure 3-23 Model D5 Contact Pressure Results, 49.825 in. Radius

a,c,e

Figure 3-24 Model F Contact Pressure Results, 4.016 in. Radius

a,c,e

Figure 3-25 Model F Contact Pressure Results, 11.722 in. Radius

a,c,e

Figure 3-26 Model F Contact Pressure Results, 20.498 in. Radius

a,c,e

Figure 3-27 Model F Contact Pressure Results, 30.193 in. Radius

a,c,e

Figure 3-28 Model F Contact Pressure Results, 48.613 in. Radius

a,c,e

Figure 3-29 Model F Contact Pressure Results, 58.308 in. Radius

3.3.11 Mean H* Calculations

Based on the calculated contact pressures for each radius, it is then possible to calculate a mean H* for each radius. The equation used is the same as in Reference 3-1 and 3-2, Equation 1-3. Table 3-20 contains the end cap loads used to determine the H*'s along with the contact pressures.

Equation 1-3 from References 3-1 and 3-2 is used to generate the cumulative pull out load throughout the thickness of the tubesheet at each elevation. These accumulated pull out loads are determined by integrating the axial contact pressure profile using the trapezoidal rule. The mean H* value is determined by interpolating the cumulative pull out resistance curve to determine the point where the pull out resisting load equals the predetermined pull out loads for each model (References 3-1 and 3-2). Table 3-21 summarizes the mean H* values for the Model F and Model D5 SGs for the NOP and SLB conditions, as appropriate, prior to the correction for Poisson contraction of the tubes. Poisson contraction must be considered in determining the mean H* to define the critical radius because it is a physical real property of the material.

The process for calculating Poisson contraction is described in Section 3.5. While principally required to establish the final value of the probabilistic H*, it is possible for the Poisson contraction correction to affect the definition of the limiting radius on the tubesheet at which the probabilistic values of H* are calculated. Table 3-22 summarizes the results of the mean H* calculations after correction for Poisson contraction. The critical radius for the Model F is determined to be [ ]^{a,c,e} inches and that for the Model D5, [ ]^{a,c,e} inches.

The limiting tubesheet radius, for the case of the mean material condition with the addition of the Poisson correction, was determined to be the same as in the current licensing basis for the Model F SGs; however, the limiting radius for the Model D5 SGs changed to [ ]^{a,c,e} inches based on the C^2 model compared to [ ]^{a,c,e} inches in the current licensing basis (Reference 3-2). Note that in the current licensing basis for the Model D5, the H* values at [ ]^{a,c,e} inches radius and at [ ]^{a,c,e} inches radius are very nearly the same. In Table 6-23 of Reference 3-2 the mean H* value at a radius of [ ]^{a,c,e} inches was [ ]^{a,c,e} inches and the mean H* value at a radius of [ ]^{a,c,e} inches was [ ]^{a,c,e} inches, a difference of less than [ ]^{a,c,e} inch. Thus, it is reasonable that application of a different structural model, the C^2 model, could result in this change in critical radius. The sensitivity of H* at both radii is also likely to be similar to the H* values at the [ ]^{a,c,e} inch TS radius. Therefore, the currently developed sensitivities for H* at the [ ]^{a,c,e} inch TS radius can be applied to the H* values calculated at the [ ]^{a,c,e} inch TS radius.

The limiting operating condition for H* is the operating condition that produces the most conservative (i.e., longest) predicted mean H* depth. The operating conditions considered were normal operating condition at low temperature (average conditions), NOP or $NOP_{LOW\ TAVG}$ and main steam line break, SLB, consistent with the current licensing bases for the limiting Model F plant (Millstone Unit 3) and the limiting Model D5 plant (Byron/Braidwood Unit 2). From Table 3-22, it is concluded that, for the Model F SGs, the limiting operating condition is NOP and for the Model D5, the limiting operating conditions is SLB.

3.3.12 Axial Location of Departure from Zero Contact Pressure

The H* distance is determined by integration of the axial contact pressure distribution from the top of the tubesheet through the thickness of the tubesheet to establish the distance required to equilibrate the applied pull out forces. Historically, nine axial locations have been considered through the thickness of the tubesheet to define the contact pressures. These points are assumed to be linearly connected to facilitate the integration for H*. Application of the C^2 model resulted in a distance of zero contact pressure at the top of the tubesheet and a relatively long span between the last zero contact pressure point and the first non-zero contact pressure point. If the distance between the first non-zero contact pressure point and the last zero-contact pressure point is large, different assumptions can be made regarding the slope of the first non-zero segment of the contact pressure profile, leading to uncertainty regarding the value of the H* distance. To address this issue, the number of axial points for calculating contact pressure was increased to provide better definition of the profile near the zero contact pressure point. For the Model F, the number of axial points was increased from nine to twelve, and for the Model D5, the number of axial points was increased from nine to thirteen for the NOP and SLB conditions. The axial distance between the last zero contact pressure point and the first non-zero contact pressure point is approximately 2.0 inches at the critical radius for the Model F, 20.498 inches (Figure 3-26). At the critical radius for the Model D5, 18.193 inches (Figure 3-20), the axial separation between the last zero contact pressure point and the first non-zero contact pressure point is approximately 2.5 inches. Between these points, respectively, the contact pressure is very low; thus, even if a steeper slope of the contact pressure profile were assumed, the effect on H* would be negligible. Therefore, it is concluded that the number of elevations utilized for contact pressure calculations accurately represent the contact pressure profile and assumptions of different slopes to the zero contact pressure point will have insignificant impact on the calculated value of H*.

3.3.13 Circumferential Contact Pressure

The contact pressure reported for each tubesheet elevation is the circumferential average of the contact pressure along the tube and tubesheet contact surface (i.e., the outer surface of the tube and the inner surface of the tubesheet tube bore). The average contact pressure along the contact surface is defined as taking the sum of the nodal normal stress in the radial direction and dividing by the number of nodes along contact surface. Figures 3-30 through 3-35 show examples of the circumferential contact pressure at the contact surface used in defining the average contact pressure in the H* analysis for the critical radius, the minimum radius and the maximum radius. The figures show the contact pressures at each node on the interface between the tube and the tubesheet based on the C^2 model results. The typical variation in amplitude for the circumferential distribution of contact pressure is on the order of 500 psi. The reported non-zero average contact pressure at an elevation accounts for the variation in contact pressure as a function of circumferential position. Therefore, the variation in contact pressure around the circumference of a tube is not great enough to generate a leakage channel. For the Model F, at the critical radius [ ]^{a,c,e} inches, the first non-zero contact pressure point is defined at approximately 2.0 inches below the top of the tubesheet (see Figure 3-25, NOP condition). From Figure 3-30 it is seen that the predicted contact pressures at less than 4 inches below the top of the tubesheet appear to oscillate around zero.

For the Model D5, at the critical radius, [ ]^{a,c,e} inches, the first non-zero contact pressure point is defined at approximately 6.0 inches (see Figure 3-21, SLB condition). From Figure 3-33 it is seen that the predicted contact pressures at less than 8.5 inches below the top of the tubesheet appear to oscillate around zero. However, the net average contact pressure is slightly greater than zero (see Table 3-11). The variations about the mean contact pressures are artifacts of the model and its convergence criteria.

Because the model is a quarter symmetry model, and because the contact pressures at all non-zero contact pressure elevations are positive, it is concluded that positive contact pressure exists circumferentially around the tube at the non-zero contact pressure elevations for the Model F and Model D5 SGs.

Table 3-20 H* Input Summary
(References 3-1 and 3-2)

	NOP	SLB
SG Model/Tube OD[1]	**End Cap Load (lb)**	**End Cap Load (lb)**
D5/[ ]^{a,c,e}		
F/[ ]^{a,c,e}		

a,c,e

Notes:
1. Maximum tubesheet bore diameter.
2. End cap loads based on 3ΔP for H* structural analysis.

Table 3-21 Summary of H* Mean Values before Poisson Correction
(All dimensions in inches)

SG Model	Radius	NOP H* a,c,e	SLB H*
F	4.016		(1)
	11.722		
	20.498		
	30.193		
	48.613		
	58.308		a,c,e
D5	4.437	(2)	
	10.431		
	18.139		
	26.703		
	42.974		
	49.825		

Notes:
1. The limiting condition for the Model F SG is NOP based on Reference 3-1.
2. The limiting condition for the Model D5 SG is SLB.

Table 3-22 Summary of H* Mean Values after Poisson Correction
(All dimensions in inches)

SG Model	Radius	NOP H*	SLB H*
F	4.016	[a,c,e	(1)
	11.722		
	20.498		
	30.193		
	48.613		
	58.308	] a,c,e	
D5	4.437	(2)	[
	10.431		
	18.139		
	26.703		
	42.974		
	49.825		]

Notes:
1. The limiting condition for the Model F SG is NOP based on Reference 3-1.
2. The limiting condition for the Model D5 SG is SLB.

a,c,e

Figure 3-30 Model F: Circumferential Contact Pressure at the Critical Radius

a,c,e

Figure 3-31 Model F: Circumferential Contact Pressure at the Minimum Radius

a,c,e

Figure 3-32 Model F: Circumferential Contact Pressure at the Maximum Radius

a,c,e

Figure 3-33 Model D5: Circumferential Contact Pressure at the Critical Radius

a,c,e

Figure 3-34 Model D5: Circumferential Contact Pressure at the Minimum Radius

a,c,e

Figure 3-35 Model D5: Circumferential Contact Pressure at the Maximum Radius

3.4 CALCULATIONS OF PROBABILISTIC H* USING THE C^2 MODEL

Development of the probabilistic value of H* for the current licensing basis, is documented in References 3-1, 3-2 and 3-11 based on application of the thick shell equations. The variability surface was developed for the key variables that influence H*, the tube and tubesheet coefficients of thermal expansion (CTE) in those analyses. This surface was randomly sampled using a Monte Carlo approach, and from this, the probabilistic values of H* were determined. Development of the variability surface was straightforward because the application of the thick shell equations enabled rapid solutions for H* over a large number of input parameter variations.

Application of the square cell (C^2) model to develop the variability surface poses a significant challenge because calculation of the H* values requires an extremely large number of calculations with both the 3-D FEA tubesheet model and the square cell model. Therefore, a simplified approach was employed that utilizes the prior variability results from the thick shell model to reduce the number of additional analyses required with the C^2 model. This approach is justified because both the thick shell model and the square cell model represent identically the same structure. The same structure with the same material properties must respond to variations in input parameters in the same manner, regardless of which analytical model is used to represent it. The detailed responses from separate models are expected to be different but the general trend of the response must be the same.

In References 3-1, 3-2 and 3-11, it was determined that the limiting values of H* occur when the variation of the tubesheet CTE is greater than its mean value in conjunction with variation of the tube CTE less than its mean. This relationship must hold true for maximum values of H* regardless of which analytical model is applied. Therefore, it is possible to define a reduced data set for application of the C^2 model using the results of the thick shell model as a guide. Further, the specific combinations of the tube and tubesheet CTEs that lead to the required probabilistic values of H* should be essentially the same regardless of which analytical model is employed.

The Monte Carlo simulation process by which the distribution of H* is computed for a given CTE response surface is described in Reference 3-11 for application of the thick shell model. The analyses described in this section address the relative behavior of the square cell and thick shell models in the local region of CTE space (tube-CTE and tubesheet-CTE) that leads to the 95th percentile value of H*.

The C^2 model is a structural model which replaces the thick shell equation approach of References 3-1 and 3-2 used to determine the contact pressure distribution between the tube and the tubesheet that are used to calculate H*. The results of using the C^2 analysis confirm the prior results using the thick shell model; that is, that mean and probabilistic values for H* are defined within the span of the tubesheet. As expected, the H* values predicted using the C^2 model are somewhat different than those predicted by the thick shell model. The difference between the models reflects, in part, the difference in the models and also the changes to the 3-D FEA model discussed in Section 3.2 and Section 3.3 which resulted in updated tubesheet displacements and contact pressures. The C^2 model is described in Section 3.3 of this report.

3.4.1 Assumptions

The assumptions made for the structural analyses of the tubes and tubesheet also apply to the analysis of the probabilistic value of H*. Sections 3.1 through 3.3 of this report provide a description of those assumptions.

3.4.2 Methods Discussion

3.4.2.1 General Methodology

It is not practicable to determine the sensitivity of H* to variations of the significant variable (tube and tubesheet CTEs) over a large domain using the C^2 model. Therefore, the structural response variability surface, as documented in the current licensing basis, i.e., Figure 8-5 in References 3-1 and 3-2, is used as the basis for determining the combinations of these variables that lead to the high probability values of H*. It has been determined that the high probability values of H* always occur when the tube CTE varies negatively from its mean and the tubesheet CTE varies positively from its mean. As noted above, this conclusion is independent of the model used to represent the same physical structure. Consequently, the gross response of the structure to variations in the significant input parameters will be the same. For example, it must be true that the maximum probabilistic value of H* will occur when the tubesheet CTE varies from its mean in a positive manner and when the tube CTE varies from its mean in a negative manner. The mean values of CTEs for the tube and the tubesheet and their respective standard deviations ([ ]^{a,c,e} % for the tube material CTE and [ ]^{a,c,e} % for the tubesheet material) are taken from References 3-1, 3-2, and 3-17.

The results of Monte Carlo sampling from the response surface defines the specific combination of the significant variables that lead to the high probability values of H*, because the specific input values of the variables are saved along with the values of H*. The results for the upper 10% tail of the H* distribution (e.g., rank order 9000 to rank order 10,000 in 10,000 simulations) from the licensing basis analysis were output as a 4 column by 1000 row matrix. The values in the matrix are the rank order statistic (i.e., 9001 to 10000), the H* value at the given rank order, the variation in the tubesheet CTE about its mean value in terms of $m\sigma_{TS}$, and the variation in the tube CTE about its mean value in terms of $n\sigma_T$ where m and n are the multipliers (positive or negative) on standard deviations added to the mean value of the respective CTEs (see Table 3-23).

For the range of multipliers m and n on the tubesheet and tube CTE standard deviations, respectively, shown on Table 3-23, the absolute values for the CTEs used in the analysis are shown on Table 3-24 for the tubesheet material and on Table 3-25 for the tube material. The result of using the material properties in Table 3-24 in the finite element analysis of the lower SG complex is the tubesheet displacement as a function of elevation. This result, along with the variation in the tube properties described in Table 3-25 are used as input to the square cell analysis.

"Break Line" Approach

The individual CTEs that result in the desired probabilistic values of H* can be combined into a single variable, which is the square root of the sum of the squares of the individual CTE values for the tube and tubesheet (shown as the last column in Table 3-23). This approach was originally documented in

Reference 3-11. The typical range of values for the combined variable for H* rank orders between 9,000 and 10,000 is between three and six for all steam generators.

Figure 3-36 shows the typical relation between the combined significant variables and the H* values above the 90th percentile from the licensing basis analysis for a SG candidate for H*. (The results in Figure 3-36 are taken from the analysis of the Model D5 SG.[1]) The figure illustrates that the rank order points of interest all fall above a very well defined line. The lower bound of the data is termed the "break line." The break line is the maximum value of H* for a constant value of "alpha," the combined significant variables affecting H*. Therefore, the break line contains the limiting H*. The "break line" can be fit using the data points that define the lower bound of the data; however, experience has shown that the fit is essentially linear. In this application, the linear fit was used.

Because the value of the combined significant variables are taken directly from the rank ordered results from the original analysis, the break line can also be defined in terms of the rank order instead of H* values. Figure 3-37 shows the break line defined by the rank order of the points selected.

The break line is used to determine specific combinations of the tube and tubesheet CTE to be used in a series of structural analysis cases using both the 3-D FEA model and the C^2 model. For example, if a specific rank order H* estimate is desired, say the 9500th, the matrix of data from the upper 10% of the Monte Carlo Analysis based on the thick shell variability analysis is entered and the specific values of CTE for the tube and the tubesheet are selected that correspond to the desired rank order.

The values of tube and tubesheet CTE used in the C^2 analysis were selected based on the required rank order statistics that met the probabilistic goals for H*. For example, the 95th percentile H* estimate at the 50th percentile confidence interval, corresponds to a rank order statistic of 9500 out of 10000 trials. The selected values typically fall on the break line, but, in the case where a specific rank order is required to meet a higher probabilistic estimate and confidence value (i.e., 95/95), the exact CTE properties at the required (or bounding) rank order were selected except as discussed below.

When used in the C^2 analysis, the specific values of tubesheet CTE are always greater than the mean and the specific values of tube CTE are always less than the mean. Because of the nature of Monte Carlo process, and because, for each 10,000 simulation set, only one tubesheet is assumed, it is possible for the upper 10% of the rank ordered simulations to include CTE combinations in which the tubesheet CTE varies negatively but is compensated for by a very large negative tube CTE variation. For example, suppose that at a given required rank order, the combination of tube and tubesheet CTE resulted in a

1. Although based on the same data, Figure 3-36 is characteristically the same but different in detail than Figure 3-32 in Rev. 0 of this report. Both figures are correct but they represent different steps in the calculation process. Because only one tubesheet is represented in the Monte Carlo sampling from the uncertainty surface, half of the 10,000 samples reflect negative variations of the tubesheet CTE. When the tube and tubesheet variables are combined to form the "alpha" term, the sign of the negative TS CTE variation is lost, and the "alpha" value is fictitious for those cases. While only a few percent of these combinations of CTE's are among the top 10% of the rank ordered statistic, those cases do result in upward scatter in Figure 3-32 in Revision 0 of this report; however, they must be included to properly represent the top 10% of the rank ordered Monte Carlo results. Figure 3-36 in this report shows the same data but without the points that have negative values of tubesheet CTE variation. These points were removed because there is no sensitivity data for negative TS variations in H* values among the top 10% of 10,000 Monte Carlo simulations.

negative (decreasing) variation on the tubesheet, but an exceedingly large (greater than -4σ) variation on the tube CTE. Such a combination of material properties at that rank order was rejected as being practically unrealistic in favor of a rank order close to (greater than) the required rank order value with a positive tubesheet CTE variation and a smaller negative tube CTE variation. It is shown below that this choice does not result in significant variations in H*.

The opposite case, in which a positive tube CTE value may be selected that is compensated for by a very large positive tubesheet CTE, does not occur because, given the large number of tubes that are sampled, the probability of this case occurring is exceptionally small. While theoretically possible, cases like this have not been experienced in the probabilistic analysis of H*.

The rank orders and CTE values used in the C^2 H* analysis are always selected so that they bound the rank order required to meet the stated probabilistic goals for H* (e.g., 95/50 or 95/95) and so that the actual rank order value can be interpolated from the analysis results if necessary (Figure 3-38). In order to accommodate that goal, it is sometimes necessary to use CTE values that do not fall directly on the break line. Use of the tube and tubesheet CTE data that varies from the break line is not a concern because the variation in H* for the licensing basis response surface (using the thick shell equations) about a given point at a specified rank order is less than 2% of the value of H*, on the order of 0.10 inch or less. Figure 3-39 and Figure 3-40 show the typical variation in H* over a range of CTE combinations ("alpha") for the bounding rank orders in the Model F NOP and Model D5 SLB response surface from Reference 3-1 and Reference 3-9.

The expected variation from a linear fit over the required range of rank order values is less than 0.20 inch regardless of CTE value in the Model F SG. The expected variation from a linear fit over the required range of rank order values is less than 0.10 inch regardless of CTE value in the Model D5 SG. A similar analysis using the C^2 model has shown that the same level of small variation (on the order of 0.05 inch or less) occurs with different combinations of CTEs at about the same rank order. Table 3-29 shows the H* results using C^2 data from the Model F NOP analysis results at approximately the 95th percentile probability and 95th percentile confidence rank order. Therefore, it is concluded that a range of CTE combinations in a narrow band of order statistics will produce no significant changes in the resulting value of H* for both the thick shell and C^2 models and that the use of the input variables associated with specific order statistics based on the thick shell model will produce consistent results when applied in the C^2 model.

Higher Confidence Limits

The order statistic for higher confidence intervals (e.g., 95%) is calculated using a method described in Reference 3-12. This method involves calculating the run-to-run variance in Monte Carlo order statistics and calculating a bounding order statistic to ensure a higher confidence. The run-to-run variance is

$$\sigma^2 = np(1-p) \qquad \text{(Equation 3-7)}$$

Where n is the number of trials and p is the desired probability level. For 10,000 trials and a probability of 95%, the run-to-run standard deviation is 22. For a confidence of 95%, the appropriate adjustment factor of 1.645 is multiplied by this value, giving an adjustment of 36. Therefore, the appropriate order statistic for 95/95 is 9536 (9500+36). In order to ensure that the final result is attained at 95% confidence, other

sources of uncertainty must be bounded at 95% confidence. In this analysis, the other sources of uncertainty are the tube and tubesheet CTE standard deviations. Work documented in Reference 3-17 has shown that the values for the tube and tubesheet standard deviation for CTE conservatively bound 95% confidence values. Therefore, a high-confidence value can be obtained by simply moving to a higher order statistic by the method described above.

Whole Plant Analysis

The rank orders from 10,000 simulations required to meet the probabilistic H* values for each of the limiting plants in the H* fleet are listed in Table 3-26. The difference in the required order statistic for the whole bundle H* estimates and the whole plant H* estimates is based on the population of the tubes in the plant. The number of tubes in a plant depends on the SG model and the number of SGs in a plant. For simplicity, the entire design population of tubes, including currently plugged tubes, is considered.

The difference between a whole bundle value of 9,500 (95/50) and a whole plant value is defined by the 9,500th H* value for the combined results of 10,000 simulations of each SG in the plant. For example, consider a 4-loop plant: Performing the 10,000 trial Monte Carlo simulation four times to represent four different generators yields four different sets of rank ordered vectors in terms of H*, TS CTE variation and T CTE variation. All four vectors will be similar, but yield slightly different H* values at the same rank order. A fifth vector is then produced whose i^{th} element consists of the maximum H* among the i^{th} elements of the four beginning vectors. This vector is then sorted, and the rank order statistic for 95/50 is the 9,500th value of H* for the whole plant. This value of H* is then searched for in an ordered input vector to determine approximately what rank order statistic for a single steam generator corresponds to the 9,500th rank order H* for an entire plant.

To apply the method discussed herein, it is necessary to identify the whole bundle rank order of the H* value that is the same as the 95% H* value for the whole plant. For example, the value of the 95% H* for the four SGs in a Model F plant is equivalent to the [ ]^{a,c,c} H* value for a single Model F bundle. Other plants have different SG populations than those using the Model F SG; therefore, the equivalent rank order for the different model SG will also be different. The difference between the whole bundle H* value and the whole plant H* value comes from using the tube and tubesheet CTE values associated with the H* value for the whole plant 95% in the calculations using the C^2 model.

The specific rank order points selected for each of the limiting plants in the H* fleet are listed in Table 3-27.

The selected values of the tubesheet CTE are used in a 3-D finite element analysis of the lower SG complex. The structural model, analysis method, assumptions and inputs to the lower SG complex analysis are the same to those described in References 3-1 and 3-2 but modified as discussed in Section 3.2 of this report. The resulting tubesheet displacements calculated from the model using the increased tubesheet CTE, with the matching decreased tube CTE properties, become inputs to the square cell model, which calculates the contact pressures for the specific combination of tube and tubesheet CTE applied. The resulting contact pressures are then used to calculate the value of H* for that combination of tube and tubesheet CTE. This process is repeated for each of the selected data points along the break line.

The H* values for the same values of rank order statistic in the licensing basis and the square cell analysis are directly compared by plotting the resulting H* values as a function of the rank order statistic. Figure 3-38 shows the results based on the NOP condition analysis for the Model F SG. It is observed that in the rank order range of interest, the results are well approximated by a straight line. It is further observed that the value of H* is increased based on the C^2 model compared to the thick shell model. As noted previously, this difference is the result of application of the more accurate C^2 model in conjunction with modified displacement results from the updated 3-D FEA model of the tubesheet region (see Section 3.1).

Figure 3-38 can be used to interpolate the H* value of the rank order statistic based on the required rank order given in Table 3-26 for each of the models of SG. For the current application, C^2 model analyses were performed for the specific CTE inputs associated with the desired rank order statistic.

That the H* values calculated using the new inputs to the square cell model correspond closely to the rank order statistic from the licensing basis was verified by considering points on the break line adjacent to the selected points. Adjacent points often exhibit significant difference in the CTE values for the tube and tubesheet compared to a selected point. This is shown on Table 3-28 which shows the variations among the CTEs for a typical range of rank order results selected at random from among the results of the Monte Carlo analyses performed for the current licensing basis. More specifically, when a narrow range of rank order results is considered, as shown on Table 3-29, consideration of adjacent point input values to the C^2 model yielded essentially the same results. The H* results for any given rank order may vary slightly from one point to the next but the absolute difference in the predicted H* value is less than 0.10 inch. This confirms that the process of defining input values for the C^2 model from the Monte Carlo results based on the thick shell model is a valid approach and that the probabilistic H* results based on the C^2 model are in close agreement with the rank order statistics based on the thick shell model. This is an important result because it shows that the general trends and conclusions from the prior thick shell model analysis apply to the C^2 output. The specific trend that the comparison between the C^2 result and the thick shell result shows is that in the probabilistic region of interest the response surface can be approximated by a linear slope.

Final H* Calculation Process

The H* results from the licensing basis analysis include the effect of the tubesheet thermal distribution offset, and a 0.30 inch distance is added to address potential uncertainty in the location of the bottom of the expansion transition (BET) at the top of the tubesheet (TTS) but do not include the adjustment for crevice pressure or any benefit from the installation process (e.g., residual contact pressure). Section 6.4.5, Section 6.4.8, and Section 8.1.1 in References 3-1 and 3-2 discuss the effects of crevice pressure and the reasons for adjusting the final tube length in the H* calculation process. The crevice pressure adjustment is discussed in Section 3.6. The final H* value for the desired rank order statistic is the H* value obtained from the interpolation of the bounding H* values plus the crevice pressure adjustment as discussed in Section 3.6.

3.4.2.2 Independent Validation of Method

To further confirm that the approach discussed above, that is, to use the significant variable combinations for desired rank order statistic from the thick shell model analysis as input to the C^2 analysis, an

independent analysis was performed which confirmed the C^2 model approach used. Reference 3-16 documents an approach based on differential thermal expansion; i.e., the combination of tube and tubesheet CTE that yield high confidence H* values. Reference 3-16 showed by independent approach that the break line approach is reasonable and correct.

3.4.3 Application to Bounding Model F SG (Millstone Unit 3)

The general approach to the probabilistic analysis for H* is applied for all models of SGs that are candidates for H*. For the Model F (Millstone Unit 3) SGs, there are no exceptions that are required to this process. Because the limiting condition for the Model F is NOP, it is necessary to perform the analysis for the whole plant complement of tubes because all loops are subject to the NOP conditions.

The necessary inputs for the probabilistic analysis using the C^2 model for the Model F SG are:

- The limiting operating condition for H*. The limiting operating condition for the Model F SGs was determined to be the NOP condition.
- The limiting radius for H* for the Model F SGs, which is [ ]^{a,c,e} inches.

Based on the Monte Carlo (MC) sampling results, the definition of the break line for the Model F SGs (Figure 3-41) in the upper 10% of the rank order is characteristically the same as that shown in Figure 3-37. Figure 3-42 shows the same data as Figure 3-41 but plotted as H* against the combined tube and tubesheet CTE values in the range of interest for the probabilistic H*. The three points shown as open symbols on Figure 3-42 are the points selected for the Model F SGs as shown on Table 3-30. Figure 3-43 is a plot of H* versus the selected rank order values.

3.4.3.1 Model F (Millstone Unit 3) Results

The H* values (without the crevice pressure adjustment) from the contact pressure distributions developed using the C^2 model at the limiting TS radius are shown in Table 3-30 together with the rank order of the input values as discussed above. Also shown is for comparison is the raw H* value from the reference analysis of Reference 3-1. The H* estimates based on the C^2 model results are about two to three inches greater than those from the current licensing basis. The results shown in Table 3-30 are represented graphically in Figure 3-43 for both the reference analysis and for application of the C^2 model.

Although the values of H* at the required rank orders of interest were calculated directly with the C^2 model using the CTE inputs corresponding to those rank orders, Figure 3-43 provides an example of how the break line concept can be applied for other rank orders of interest. The linear fit used to interpolate the value of H* at the desired rank order statistic for the Model F is given by:

$$H^*_{RO} = [\quad]^{a,c,e}$$

where,

RO = the desired Rank Order statistic between 9694 and 9890.

3.4.4 Application to Bounding Model D5 SGs (Byron/Braidwood Unit 2)

The general approach to the probabilistic analysis for H* is applied for all models of SGs that are candidates for H*. The exceptions to the process discussed in Section 3.4.2 for the probabilistic analysis based on the C^2 model for Byron/Braidwood Unit 2 are:

1. The limiting condition for H* is SLB, therefore, the direct use of the existing Model D5 response surface from Reference 3-2 is not appropriate. A reduced response surface was calculated, utilizing the thick shell methodology discussed in Reference 3-2, to establish input conditions for the C^2 analysis for the Model D5 SLB conditions [Reference 3-9].

2. It is not necessary to perform a "whole plant" analysis because the limiting conditions for the Model D5 SGs are the SLB conditions. Only one loop is affected during a SLB accident.

The necessary inputs for the probabilistic analysis using the C^2 model for the Model D5 SGs are:

- The limiting operating condition for H*. The limiting operating condition for the Model D5 SGs was determined to be the SLB condition.

- The limiting radius for H* for the Model D5 SGs. The limiting radius for Byron/Braidwood Unit 2 is [ ]^{a,c,e} inches. All other structural models and inputs are the same as discussed in Reference 3-2 including the range of significant material properties, CTEs for the tubesheet and tube material.

The response surface for the Byron/Braidwood Unit 2 SGs for the SLB condition was developed using the thick shell model for the input specific to the Byron/Braidwood Unit 2 SLB conditions. A reduced analysis matrix was defined for the C^2 model based on the experience from prior sensitivity analyses using the thick shell model. As noted above, the limiting values of H* always occur when the tubesheet CTE varies positively from its mean and the tube CTE varies negatively from its mean. Accordingly, a range of tubesheet CTEs and tube CTEs was chosen to define the reduced response surface for subsequent sampling by the Monte Carlo process. These variations of the CTEs are consistent with the ranges of variations previously identified as including the combination that results in the maximum H* value.

Based on the MC sampling results, the definition of the break line (Figure 3-44) in the upper 10% of the rank order is characteristically the same as that shown in Figure 3-37. The details of the response surface are different because the limiting loading condition for Byron/Braidwood Unit 2 is the postulated SLB condition. Both the pressure and temperature input during SLB are different than those for NOP conditions, leading to a different structural response.

Figure 3-45 shows the same data as Figure 3-44 but plotted as H* against the Monte Carlo rank order in the range of interest for the probabilistic H*. The three points shown as open symbols on Figure 3-44 are the points selected for the Model D5 SGs as shown on Table 3-30.

3.4.4.1 Model D5 (Byron/Braidwood Unit 2) Results

The H* values (without the crevice pressure adjustment) from the contact pressure distributions developed using the C^2 model at the limiting TS radius are shown in Table 3-30 together with the rank order of the input values as discussed above. The results shown in Table 3-30 are represented graphically in Figure 3-46. The results from the C2 model are approximately 2 inches less than the results from the Reference 3-2 analysis, but are characteristically the same.

Although the values of H* at the required rank orders of interest were calculated directly with the C^2 model using the CTE inputs corresponding to those rank orders, Figure 3-46 provides a second example of how the break line concept can be applied for other rank orders of interest. The linear fit used to interpolate the value of H* at the desired rank order statistic for the Model D5 is given by:

$$H^*_{RO} = [\qquad\qquad\qquad\qquad\qquad\qquad]^{a,c,e}$$

where,

RO = the desired Rank Order statistic between 9149 and 9536.

The final values for the Model D5 H* at different probabilities and confidence estimates using the C^2 model are different from the Model D5 H* values in WCAP-17072-P, because the boundary conditions during NOP (Reference 3-2) are different from the boundary conditions applied to the models during SLB (current analysis). For example, the temperature of the tubesheet during SLB (Primary Fluid Temperature = [ ]^{a,c,e}°F) is lower than the temperature of the tubesheet during NOP (Primary Fluid Temperature = [ ]^{a,c,e}°F), which results in smaller tubesheet displacements. The end cap load used to calculate H* during SLB ($1.4\Delta P_{SLB}$ = [ ]^{a,c,e} lbf) is also less than the end cap load used to calculate H* during NOP ($3.0\Delta P_{NOP}$ = [ ]^{a,c,e} lbf). The net effect is that the SLB results use a different contact pressure distribution that is less sensitive to variations in CTE even though the mean H* value for SLB condition is larger than the mean NOP H* value.

Table 3-23 Typical Monte Carlo Result Output

Rank #	HSTAR	$n\sigma_T$[1]	$m\sigma_{TS}$[1]	Alpha
9000				
9001				
9002				
9003				
9004				
9995				
9996				
9997				
9998				
9999				
10000				

a,c,e

Note:
1. $n\sigma_T$ is the multiplier on σ for the tube; $m\sigma_{TS}$ is the multiplier on σ for the tubesheet.

Table 3-24 Positive Variations About the Mean TS CTE Used for FEA (Units of 10^{-6} in/in/°F)

	Multiplier on Standard Deviation						
Temp. °F	Mean						
70	6.50						
200	6.67						
300	6.87						
400	7.07						
500	7.25						
600	7.42						
700	7.59						

a,c,e

Table 3-25 Negative Variations About the Mean Tube CTE Used for FEA (Units of 10^{-6} in/in/°F)

Temp. °F	Mean	Multiplier on Standard Deviation										
212	7.22											
300	7.40											
420	7.60											
500	7.70											
600	7.82											
628	7.85											

a,c,e

Table 3-26 Required Probabilistic Estimate for H*

Model SG	Whole Bundle Estimate		Whole Plant Estimate	
	95/50	95/95	95/50	95/95
F	9500	9536		
D5	9500	9536		
44F	9500	9536		
44F 2-Loop	9500	9536		
51F	9500	9536		

a,c,e

Notes:
1. Whole plant does not apply because SLB is the limiting condition for H*.
2. Values are the whole bundle rank orders based on whole plant rank order equivalent H* to recover the corresponding values of tube and tubesheet CTE.

Table 3-27 Monte Carlo Data Used in Comparative Probabilistic Analysis

Model SG	Limiting Operating Condition	Rank Order Statistic (1)	Tubesheet CTE Variation (standard deviations)	Tube CTE Variation (standard deviations)	Alpha	H* from Current Licensing Basis
F	NOP	[				
D5	SLB					
44F 3-Loop	NOP					
44F 2-Loop	SLB[2]					
51F	NOP					
		]				

a,c,e

Notes:
1. Based on 10,000 simulations.
2. Point Beach specific H* values did not exist in the previous licensing basis.

Table 3-28 Typical Variation of CTEs Over a Range of Rank Order Statistics

Rank	H*	Tube CTE	Tubesheet CTE	"Alpha"
9880				
9881				
9882				
9883				
9884				
9885				
9886				
9887				
9888				
9889				
9890				
9891				
9892				
9893				
9894				
9895				
9896				
9897				
9898				
9899				
9900				

a,c,e

Table 3-29 Variation of H* for Adjacent Rank Order Variables (Ref. Model F C^2 Results)

	Variation Input		
MC	T CTE	TS CTE	C^2 H*
#	$n\sigma$	$m\sigma$	in.
9889			
9890			
9891			

a,c,e

Table 3-30 Model F and Model D5 H* Results
(Without P_{crev} Adjustment)

MC Rank in 10,000 Simulations	H* Results from Current Licensing Basis (Reference 3-1, 3-2)	H* Result from Square Cell Analysis
	Model F (in.)	
	Model D5 (in.)	

a,c,e

a,c,e

a,c,e

Figure 3-36 Typical Result for Plotting the Combined Tube and Tubesheet CTE Values vs. H* from the Licensing Basis Analysis (Ref. Model D5 NOP)

a,c,e

Figure 3-37 Typical Result of Combined Tube and Tubesheet CTE Values vs. Monte Carlo Rank Order from the Licensing Basis Analysis (Ref. Model D5 SLB)

a,c,e

Figure 3-38 H* Curves from Response Surface (Ref. Model F)

a,c,e

Figure 3-39 Variation in H* from a Linear Fit of H* Results in a Range of Order Statistics Required to Meet Probabilistic H* Goals (Ref. Model D5 SLB)

a,c,e

Figure 3-40 Variation in H* from a Linear Fit of H* Results in a Range of Order Statistics Required to Meet Probabilistic H* Goals (Ref. Model F NOP)

a,c,e

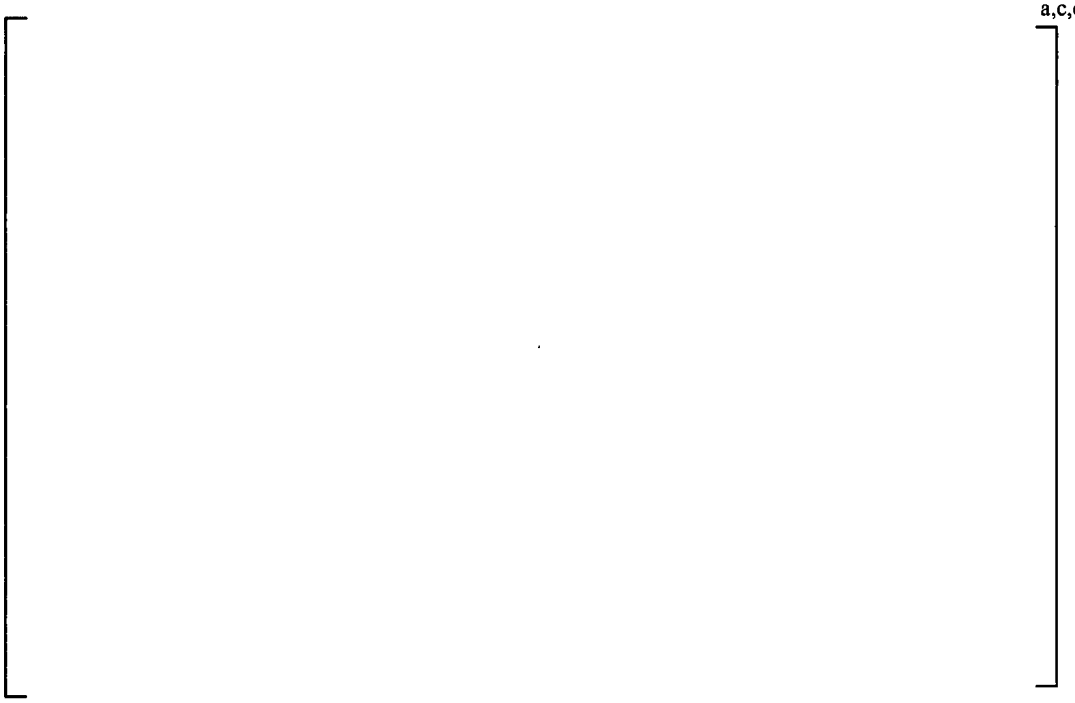

Figure 3-41 Model F NOP Combined CTE_T and CTE_{TS} vs. Monte Carlo Rank Order

a,c,e

Figure 3-42 Model F NOP Combined CTE_T and CTE_{TS} vs. H* Value

a,c,e

Figure 3-43 Model F H* Summary Showing Linear Fit Results

a,c,e

Figure 3-44 Model D5 SLB Combined CTE_T and CTE_{TS} vs. Monte Carlo Rank Order

a,c,e

Figure 3-45 Model D5 SLB Combined CTE_T and CTE_{TS} vs. H* Value

a,c,e

Figure 3-46 Model D5 H* Summary Showing Linear Fit Results

3.5 POISSON CONTRACTION EFFECT ON H*

An evaluation was performed to determine the effect of Poisson contraction of the tube on H* due to end cap loading. The pressure differential across the tube wall creates an effective end cap load, generating a positive axial stress state in the tube. This will cause a radial contraction of the tube via Poisson's ratio, which will necessarily reduce the contact pressure between the tube and tubesheet, hence increasing H*. The purpose of this section of the report is to address the impact of Poisson contraction on the values calculated for H* using the C^2 model.

3.5.1 Methods Discussion

The method used to evaluate the effect of Poisson's ratio on H* is a simplified approach using approximations to determine the reduction in contact pressure. A classical thick shell formula is used to calculate the change in radius due to Poisson's ratio effects from an applied end cap load. This change in radius is directly converted to a contact pressure utilizing the thick shell equations in References 3-1 and 3-2. This contact pressure is then subtracted from the calculated contact pressure curve and the final H* distance is calculated. All calculations for Poisson's contraction are based on an end cap load without a factor of safety, as it is unrealistic to apply a factor of safety to a physical effect such as Poisson's contraction. The end cap load used to generate H*, however, continues to include the appropriate safety factor (3.0 for 100% power, 1.4 for SLB).

3.5.2 Input

The input for this analysis consists of steam generator dimensions for the Model F and Model D5 SGs, material properties from the ASME Code, and pressure and temperature conditions for the applicable operating conditions (e.g., Model D5 SLB transient, Model F 100% Power) as defined in Reference 3-6.

The end cap load for the Model F SGs for NOP is [ ]^{a,c,e} psi. This includes a factor of safety of 3.0 on the NOP pressure differential. The end cap load for the Model D5 SGs during a postulated SLB is [ ]^{a,c,e} psi. This includes a factor of safety of 1.4 on the SLB pressure differential. The modulus of elasticity is the taken from Table 3-3. Poisson's ratio for Alloy 600 is 0.31 as taken from the ASME Code, Reference 3-10.

Material properties were taken at temperatures consistent with those used in the FEA discussed in Section 3.1. Material properties are taken at [ ]^{a,c,e} °F for NOP conditions for the Model F SGs and [ ]^{a,c,e} °F for a postulated SLB for the Model D5 SGs.

3.5.3 Calculation of Radial Dilation

From Reference 3-15 (Page 396), the radial dilation of a pressurized thick-wall cylinder is given by:

$$\Delta R = \frac{r}{E_t\left(r_o^2 - r_i^2\right)}\left[\left(1-2\nu\right)\left(p_i r_i^2 - p_o r_o^2\right)+\left(1+\nu\right)\frac{r_i^2 r_o^2\left(p_i - p_o\right)}{r^2} - \frac{\nu P}{\pi}\right] \quad \text{(Equation 3-8)}$$

where,

P = End cap load (pounds)
ν = Poisson's ratio
r = Radial coordinate (inches)
r_o = Outer radius of tube (inches)
r_i = Inner radius of tube (inches)
p_i = Pressure on inside of tube (psi)
p_o = Pressure on outside of tube (psi)
E_t = Elastic Modulus of tube (psi)
π = pi (3.14159...)
ΔR = Change in radial coordinate due to loadings (inches)

Since the figure of interest is the radial contact at the outside radius due to the applied end cap load, the difference is:

$$\Delta R_{endcap} = -\frac{r_o \nu P}{E\pi\left(r_o^2 - r_i^2\right)} \quad \text{(Equation 3-9)}$$

This equation is used to calculate radial dilations due to the Poisson contraction alone (Table 3-31). As can be seen, there is a small radial contraction (approximately [ ]^{a,c,e} micro-inches) due to Poisson effects.

3.5.4 Calculation of Contact Pressure Reduction from Poisson Effect

The contact pressure change due to Poisson effects can be estimated by using the thick shell equations from Reference 3-1. The thick shell formula is (page 6-91 of Reference 3-1): a,c,e

[ ]

(Equation 3-10)

where,

P_i = Internal primary side pressure, psi
P_{crev} = Crevice pressure, psi
r_i = Inside radius of tube, in
r_o = Outside radius of tube, in
α_t = Coefficient of thermal expansion of tube, in/in/°F
E_t = Modulus of Elasticity of tube, psi
E_{ts} = Modulus of Elasticity of tubesheet, psi
T_t = Temperature of tube, °F
ν = Poisson's Ratio of the material
$P_{contact}$ = Contact Pressure
D = Outside radius of cylinder which provides the same radial stiffness as the tubesheet

As can be seen, the thick shell equation for contact pressure is simply a sum of radial displacements divided by an effective elastic constant. This makes intuitive sense because the physical interpretation of the thick shell equations is as follows:

1. Apply internal pressure, crevice pressure, and thermal loads to a free tube which has a nominal outside diameter equivalent to the collar bore ID. Calculate the resultant radial dilation.

2. Calculate the bore displacement of a free collar from crevice pressure and the applied dilation from the 3-D FEA model.

3. If the answers to one and two above possess a geometric interference (the resultant tube radius is larger than the bore), then there exists positive contact pressure. The positive contact pressure can be calculated as that pressure which, when applied to both the tube OD and the collar ID, eliminates the geometric interference, producing line-on-line contact.

In Step 3, it is clear that the relationship between contact pressure and radial geometric interference should be linear, as the thick shell equations are linear elastic. Therefore, it is appropriate to calculate contact pressure reduction by simply dividing the differential radial displacement due to Poisson's ratio effects by the elastic constant in the denominator above:

a,c,e

[ ] (Equation 3-11)

Results of the calculation of the elastic constants are provided in Table 3-32 for the Model F and Model D5 SGs. Substituting the differential radial dilation from Table 3-31 into the above equation yields the contact pressure reductions shown in Table 3-33. As can be seen, there is a reduction of approximately ~[ ]^{a,c,e} psi at NOP conditions for the Model F and ~[ ]^{a,c,e} psi at SLB conditions for the Model D5.

The effect of Poisson contraction on H* was calculated for the critical radius because this radius determines the value of H*. In order to calculate the change in H* values due to the decreased contact pressure, the contact pressure curves from Section 3.3 must be reduced by the incremental contact pressures discussed above. The resulting contact pressure curve then must be integrated again to determine the adjusted H*. The reference square cell analysis (Section 3.3) explains the methodology for calculating H*. The formula for pull out load is

$$F = \int \mu \pi d_o P_{contact} dy \qquad \text{(Equation 3-12)}$$

Where μ is the coefficient of friction, [ ]^{a,c,c}, as discussed in References 3-1 and 3-2.

Calculations for the increased H* are shown on Table 3-34 and Table 3-35 for the Model F and Model D5, respectively. The typical adjustment to the contact pressure profile is shown in Figure 3-47. As can be seen, the contact pressure curve is shifted down by the appropriate amount. Baseline numbers are included on Table 3-34 and Table 3-35 for comparison. The increase in H* due to Poisson effects amounts to approximately [ ]^{a,c,e} inches (before attenuation). Note that Figure 3-47 contains interpolated contact pressure points to account for the attenuation distance discussed below to facilitate comparison to later calculations. These contraction values assume Poisson contraction occurs along the entire length. A more realistic calculation will account for the Poisson effect attenuating after an accumulated pull out resistance equal to the end cap load is attained. This correction is obtained by interpolation using the same methodology as for H*, but with an end cap load that does not have a factor of safety. The interpolated attenuation distance is provided in Table 3-36.

Because the axial stress in the tube goes to zero at the attenuation point, the next step in the process is to calculate new H* values with contact pressures that are reduced only inside the attenuation distance. This involves interpolating the predicted contact pressure curves from Section 3.3 and shifting only the portion of it above the attenuation point. Calculations are tabulated in Table 3-37 and Table 3-38 for the Model F and Model D5, respectively. A summary of the final H* values after adjusting for Poisson contraction and attenuation are in Table 3-39. As can be seen, the difference is [ ]^{a,c,e} inches for the Model F and [ ]^{a,c,e} for the Model D5 for the mean value of H*.

The final figure of merit is the effect that Poisson contraction has on the probabilistic H* values. Calculations for the probabilistic values are in Table 3-40 through Table 3-49. A summary of the effect of Poisson's contraction on the probabilistic values of H* is in Table 3-49. As can be seen, the effect is approximately [ ]^{a,c,e} inch for the probabilistic H* value for the Model F SG and approximately [ ]^{a,c,e} inch for the Model D5 SG.

Table 3-31 Calculation of Radial Dilation Due to Poisson Effects

Parameter	Model F NOP	Model D5 SLB
Tube R_i (in)		
Tube R_o (in)		
E_{tube} (Msi)		
End Cap Load (lbs)		
Delta-R (micro-inch)		

a,c,e

Table 3-32 Calculation of Elastic Constants

Parameter	Model F NOP	Model F SLB	Model D5 NOP	Model D5 SLB
Tube r_i (in)				
Tube r_o (in)				
Collar R_o (in)				
Tube E (Msi)				
Tubesheet E (Msi)				
ν				
Elastic Constant (in^3/lb)				

a,c,e

Table 3-33 Calculation of Reduction in Contact Pressure from Poisson Effects

Parameter	Model F NOP	Model D5 SLB
Δr due to ν (μin)	[	
Elastic Constant (in^3/lb)		
P_{con} Reduction (psi)	]	

a,c,e

Table 3-34 Baseline and Adjusted Mean H* Calculation for Model F (Millstone Unit 3) (Without Attenuation)

NOP, [ ]^{a,c,e} in. Radius					
End Cap Load = [ ]^{a,c,e} pounds					
Elevation from Bottom of Tubesheet (in)	Distance from TTS (in)	P_{con} (psi)	Accumulated Pull Out Load (pounds)	P_{con} (psi)	Accumulated Pull Out Load (pounds)
		Baseline (Unadjusted Mean H*)		H*Adjusted for Poisson Effect	
0	21.03	[			
2.00	19.03				
4.00	17.03				
6.00	15.03				
8.00	13.03				
10.52	10.515				
12.50	8.53				
15.00	6.03				
16.90	4.129				
19.03	2				
20.03	1				
21.03	0				
	H* (inches)	]			

a,c,e

Table 3-35 Baseline and Adjusted Mean H* Calculation for Model D5 (Byron/Braidwood Unit 2) (Without Attenuation)

SLB, [ ]^{a,c,e} in. Radius					
End Cap Load = [ ]^{a,c,e} pounds					
Elevation from Bottom of Tubesheet (in)	Distance from TTS (in)	P_{con} (psi)	Accumulated Pull Out Load (pounds)	P_{con} (psi)	Accumulated Pull Out Load (pounds)
		Baseline (Unadjusted Mean H*)		H*Adjusted for Poisson Effect	
0	21.03				
2	19.03				
4	17.03				
6	15.03				
8.26	12.77				
10.515	10.515				
12.5	8.53				
15	6.03				
16.901	4.129				
18	3.03				
19.03	2				
20.03	1				
21.03	0				
	H* (inches)				

a,c,e

Table 3-36 Distance for Poisson Effect to Attenuate

SG Model	F	D5
Distance for Poisson Effect to Attenuate (inches)	[ ]^{a,c,e}	[ ]^{a,c,e}

Table 3-37 Adjusted Mean H* Including Poisson Attenuation for Model F (Millstone Unit 3)

NOP 100% Power, [ ]^{a,c,e} in. Radius			
End Cap Load = [ ]^{a,c,e} pounds			
Elevation from Bottom of Tubesheet (in)	**Distance from TTS (in)**	**P_{con} (psi)**	**Accumulated Pull Out Load (pounds)**
0	21.03		
2	19.03		
4	17.03		
6	15.03		
8	13.03		
10.515	10.515		
12.5	8.53		
13.901	7.129		
15	6.03		
16.901	4.129		
19.03	2		
20.03	1		
21.03	0		
H* (inches)			

a,c,e

Table 3-38 Adjusted Mean H* Including Poisson Attenuation for Model D5 (Byron/Braidwood Unit 2)

SLB, [ ]^{a,c,e} in. Radius			
End Cap Load = [ ]^{a,c,e} pounds			
Elevation from Bottom of Tubesheet (in)	**Distance from TTS (in)**	**P_{con} (psi)**	**Accumulated Pull Out Load (pounds)**
0	21.03		
2	19.03		
4	17.03		
6	15.03		
8.26	12.77		
10.515	10.515		
10.548	10.482		
12.5	8.53		
15	6.03		
16.901	4.129		
18	3.03		
19.03	2		
20.03	1		
21.03	0		
H* (inches)			

a,c,e

Table 3-39 Comparison of Mean H* Values

Parameter	Model F (in.)	Model D5 (in.)
H* Unmodified		
H* + Poisson		
H* + Poisson + Attenuation		
Final Difference		

a,c,e

Table 3-40 Baseline and Adjusted Probabilistic H* Calculation for Model F (MC Rank 9684)

NOP, [ ]^{a,c,e} in. Radius						
End Cap Load = [ ]^{a,c,e} pounds						
Elevation from Bottom of Tubesheet (in)	Distance from TTS (in)	Baseline		Shifted due to Poisson		
		P_{con} (psi)	Accumulated Pull-Out Load (pounds)	P_{con} (psi)	Accumulated Pull Out Load (pounds)	a,c,e
0	21.03					
2.00	19.03					
4.00	17.03					
6.00	15.03					
8.00	13.03					
10.52	10.515					
12.50	8.53					
15.00	6.03					
16.90	4.129					
19.03	2					
20.03	1					
21.03	0					
H* (inches)						

Table 3-41 Baseline and Adjusted Probabilistic H* Calculation for Model D5 (MC Rank 9260)

SLB, [ ]^{a,c,e} in. Radius						
End Cap Load = [ ]^{a,c,e} pounds						
Elevation from Bottom of Tubesheet (in)	Distance from TTS (in)	Baseline		Shifted due to Poisson		
		P_{con} (psi)	Accumulated Pull Out Load (pounds)	P_{con} (psi)	Accumulated Pull Out Load (pounds)	a,c,e
0	21.03	[				
2	19.03					
4	17.03					
6	15.03					
8.26	12.77					
9.06	11.97					
10.515	10.515					
12.5	8.53					
15	6.03					
16.901	4.129					
18	3.03					
19.03	2					
20.03	1					
21.03	0					
H* (inches)						]

Table 3-42 Baseline and Adjusted Probabilistic H* Calculation for Model F

(No Attenuation, MC Rank 9890)

NOP, [ ]^{a,c,e} in. Radius						
End Cap Load = [ ]^{a,c,e} pounds						
Elevation from Bottom of Tubesheet (in)	Distance from TTS (in)	Baseline		Shifted due to Poisson		
		P_{con} (psi)	Accumulated Pull Out Load (pounds)	P_{con} (psi)	Accumulated Pull Out Load (pounds)	a,c,e
0	21.03					
2.00	19.03					
4.00	17.03					
6.00	15.03					
8.00	13.03					
10.52	10.515					
12.50	8.53					
15.00	6.03					
16.90	4.129					
19.03	2					
20.03	1					
21.03	0					
H* (inches)						

Table 3-43 Baseline and Adjusted Probabilistic H* Calculation for Model D5 (95/95)
(No Attenuation, MC Rank 9536)

SLB, [ ]^{a,c,e} in. Radius						
End Cap Load = [ ]^{a,c,e} pounds						
Elevation from Bottom of Tubesheet (in)	Distance from TTS (in)	Baseline		Shifted due to Poisson		
		P_{con} (psi)	Accumulated Pull Out Load (pounds)	P_{con} (psi)	Accumulated Pull Out Load (pounds)	a,c,e
0	21.03					
2	19.03					
4	17.03					
6	15.03					
8.26	12.77					
9.035	11.995					
10.515	10.515					
12.5	8.53					
15	6.03					
16.901	4.129					
18	3.03					
19.03	2					
20.03	1					
21.03	0					
H* (inches)						

Table 3-44 Distance for Poisson Effect to Attenuate Probabilistic H* Values
(inches)

Model SG	Model F	Model D5
MC Rank 9260	N/A	[ ]^{a,c,e}
MC Rank 9536	N/A	[ ]^{a,c,e}
MC Rank 9684	[ ]^{a,c,e}	N/A
MC Rank 9890	[ ]^{a,c,e}	N/A

Table 3-45 H* Calculation Including Poisson Attenuation Model F (Millstone Unit 3)

(With Attenuation, MC Rank 9684)

NOP, [ ]^{a,c,e} in. Radius			
End Cap Load = [ ]^{a,c,e} pounds			
Elevation Above Bottom of TS (in)	**Distance from TTS (in)**	**P_{con} (psi)**	**Accumulated Pull-Out Load (pounds)**
0	21.03		
2	19.03		
4	17.03		
6	15.03		
8	13.03		
8.946	12.084		
10.515	10.515		
12.5	8.53		
15	6.03		
16.901	4.129		
19.03	2		
20.03	1		
21.03	0		
H* (inches)			

a,c,e

Table 3-46 H* Calculation Including Poisson Attenuation Model F (Millstone Unit 3)

(With Attenuation, MC Rank 9890)

NOP, [ ]^{a,c,e} in. Radius			
End Cap Load = [ ]^{a,c,e} pounds			
Elevation Above Bottom of TS (in)	**Distance from TTS (in)**	**P_{con} (psi)**	**Accumulated Pull-Out Load (pounds)**
0	21.03		
2	19.03		
4	17.03		
6	15.03		
8	13.03		
8.425	12.605		
10.515	10.515		
12.5	8.53		
15	6.03		
16.901	4.129		
19.03	2		
20.03	1		
21.03	0		
H* (inches)			

a,c,e

Table 3-47 H* Calculation Including Poisson Attenuation Model D5 (Byron/Braidwood Unit 2)
(With Attenuation, MC Rank 9260)

SLB, [ ]^{a,c,e} in. Radius			
End Cap Load = [ ]^{a,c,e} pounds			
Elevation Above Bottom of TS (in)	**Distance from TTS (in)**	**P_{con} (psi)**	**Accumulated Pull-Out Load (pounds)**
0	21.03		
2	19.03		
4	17.03		
6	15.03		
8.26	12.77		
9.06	11.97		
10.515	10.515		
12.5	8.53		
15	6.03		
16.901	4.129		
18	3.03		
19.03	2		
20.03	1		
21.03	0		
H* (inches)			

a,c,e

Table 3-48 H* Calculation Including Poisson Attenuation Model D5 (Byron/Braidwood Unit 2)
(With Attenuation, MC Rank 9536)

SLB, [ ]^{a,c,e} in. Radius			
End Cap Load = [ ]^{a,c,e} pounds			
Elevation Above Bottom of TS (in)	**Distance from TTS (in)**	**P_{con} (psi)**	**Accumulated Pull-Out Load (pounds)**
0	21.03		
2	19.03		
4	17.03		
6	15.03		
8.26	12.77		
9.035	11.995		
10.515	10.515		
12.5	8.53		
15	6.03		
16.901	4.129		
18	3.03		
19.03	2		
20.03	1		
21.03	0		
H* (inches)			

a,c,e

Table 3-49 Comparison of Model F and Model D5 SG Probabilistic H* Values (inches)

	Model F			Model D5		
Parameter	Mean	Rank Order 9684	Rank Order 9890	Mean	Rank Order 9260	Rank Order 9536
H* Unmodified						
H* + Poisson						
H* + Poisson + Attenuation						
Final Difference						

a,c,e

a,c,e

Figure 3-47 Effect of Poisson Contraction on Contact Pressure; Model F

3.6 CREVICE PRESSURE ADJUSTMENT LENGTH

As discussed in References 3-1 and 3-2, the solution for H* is iterative to address the axial distribution of crevice pressure. Initially, it is assumed that a crack exists at the bottom of the tubesheet and that the crevice pressure axial distribution applies over the entire thickness of the tubesheet. The H* value predicted based on this assumption is less than the full depth of the tubesheet. Because the effective crevice length is no longer the full depth of the tubesheet, the axial distribution of crevice pressure is applied over the initial prediction of H* and a new value of H* is calculated.

For the Model F SGs, Reference 3-1 contains the crevice pressure correction curve. It is reproduced below as Figure 3-48 for convenience. When the probabilistic value of H*, corrected for Poisson contract is available, the curve is entered with that value of "initial prediction" and the necessary length adjustment is read. The adjustment is added to the "initial prediction" as defined above to develop the final value of H*.

For the Model D5, because it was determined that the SLB condition is limiting, it was necessary to develop a new curve for crevice pressure correction (the correction curve in Reference 3-2 is based on NOP conditions). However, the process for developing the correction curve was the same as discussed in Reference 3-2; only the input operating conditions were changed. It was not necessary to develop the entire curve because prior experience showed that the initial value of H* would be in a range centered on the mid-plane of the tubesheet. Therefore, a reduced set of sensitivity analyses were performed. The crevice pressure adjustment for the Model D5 SGs is shown on Figure 3-49. Application of this curve is the same as discussed above for the Model F SGs.

a,c,e

Figure 3-48 Model F Crevice Pressure Adjustment Curve

a,c,e

Figure 3-49 Model D5 Crevice Pressure Adjustment Curve

3.7 CALCULATION OF FINAL H*

After the probabilistic values of H* are determined as discussed in Section 3.4, and the correction is made for Poisson contraction of the tube to define the initial estimate of the probabilistic H* discussed in Section 3.5, the adjustment for crevice pressure distribution as discussed in Section 3.6 is made. The final probabilistic values of H*, with the corresponding crevice pressure length adjustments taken from Figure 3-48 and Figure 3-49, are shown in Table 3-50 and Table 3-51 for the Model F and Model D5 SGs, respectively.

Table 3-50 Summary of Model F Probabilistic Estimates

Description	MC Rank in 10K Simulations	H* -- C^2 (in.)	Attenuated Poisson Offset (in.)	Pcrev (in.) a,c,e	Final (in.)
Whole Bundle, 95/50	9500	[		]	14.82
Whole Bundle, 95/95	9536				14.84
Whole Plant, 95/50 (1)	9850				15.13
Whole Plant, 95/95	9890	]			15.21
(1): 95/50 Rank Order value determined from linear interpolation.					

Table 3-51 Summary of Model D5 Probabilistic Estimates

Description	MC Rank in 10K Simulations	H* -- C^2 (in.)	Attenuated Poisson Offset (in.)	Pcrev (in.) a,c,e	Final (in.)
Whole Bundle, 95/50	9500	[		]	14.00
Whole Bundle, 95/95	9536	]			14.01
Whole Plant, 95/50	NA	NA	NA	NA	NA
Whole Plant, 95/95	NA	NA	NA	NA	NA

3.8 REFERENCES

3-1. WCAP-17071-P, Rev. 2, "H*: Alternate Repair Criteria for the Tubesheet Expansion Region in Steam Generators with Hydraulically Expanded Tubes (Model F)," September 2010.

3-2. WCAP-17072-P, "H*: Alternate Repair Criteria for the Tubesheet Expansion Region in Steam Generators with Hydraulically Expanded Tubes (Model D5)," May 2009.

3-3. WTD-SM-75-072, "Temperature Distributions for Calculation of Secondary Skin Stress in D2-D3 Tubesheet Analysis," August 1975.

3-4. Report 1014982, "Divider Plate Cracking in Steam Generators: Results of Phase I: Analysis of Primary Water Stress Corrosion Cracking and Mechanical Fatigue in the Alloy 600 Stub Runner to Divider Plate Weld Material," EPRI, Palo Alto, CA; 2007.

3-5. Jaluria, Yogesh, "Computer Methods for Engineering," Taylor and Francis, 1996.

3-6. CN-SGMP-10-15, Rev. 1, "3-D Finite Element Analyses of Limiting Plants for H* with Thermal Profile," November 2010.

3-7. WNET-150, Volume 3, "Model E2, Steam Generator Stress Report, Primary Chamber Components Interactions Analysis," December 1978.

3-8. CN-SGMP-10-3, Rev. 1, "Square Cell Finite Element Analyses for Models D5, F, 44F and 51F Plants for H*," November 2010.

3-9. CN-SGMP-10-18, "H* Analysis Using Thick Shell Equations for Byron/Braidwood Unit 2 and Point Beach Unit 1 for Steam Line Break Conditions," October 11, 2010.

3-10. ASME B&PV Code, 2007 Edition, No Addenda, Section II, Part D, Subpart 2: Physical Properties Tables, Table PRD.

3-11. LTR-SGMP-09-100 P-Attachment, Rev. 1, "Responses to NRC Request for Additional Information on H*; Model F and Model D5 Steam Generators," September 2010.

3-12. *Statistics, Probability and Reliability for Civil and Environmental Engineers*, Kottegoda, N.T., Rosso, R., McGraw-Hill, © 1997.

3-13. Westinghouse Drawing 1105J05, Rev. 3, "Tube Plate Drilling."

3-14. LTR-SGMP-10-135, "Assessment of Feedwater Line Break Conditions on Contact Pressures for Model F for H*," October 26, 2010.

3-15. *Advanced Mechanics of Materials*, Boresi, Arthur P and Schmidt, Richard J, Sixth Edition, John Wiley and Sons Publishing.

3-16. LTR-SGMP-11-40, "Calculation of Required Parameters for Extreme H* Values," May 6, 2011.

3-17. LTR-SGDA-11-87, "High-Confidence Variances for Tube and Tubesheet CTE for H*," May 5, 2011.

3-18. LTR-SGMP-10-34, Rev. 2, "An Assessment of the Impact of Revised Normal Operating Conditions on the Catawba Unit 2 H* Calculations," April 27, 2010.

4 C² MODEL LEAKAGE INTEGRITY DISCUSSION

The model for leakage applied in References 4-1, 4-2 and 4-3 is the Darcy formulation for leakage through a porous medium. The Darcy equation is:

$$Q = \frac{\Delta p}{12 \mu K l} \qquad \text{(Equation 4-1)}$$

where,

Δp	=	the driving potential (primary to secondary pressure difference)
μ	=	the fluid dynamic viscosity
K	=	the loss coefficient for flow through the porous medium
L	=	the length of the porous medium

The Darcy formulation (Eq. 4-1) is used in References 4-1, 4-2 and 4-3 to develop the ratio of leak rates between postulated accident induced conditions and normal operating conditions (NOP). The resulting Darcy flow equation ratio can be separated into four "subfactors" as follows:

$$\frac{Q_{DBA}}{Q_{NOP}} = \frac{\Delta p_{DBA}}{\Delta p_{NOP}} \frac{\mu_{NOP}}{\mu_{DBA}} \frac{K_{NOP}}{K_{DBA}} \frac{l_{NOP}}{l_{DBA}} \qquad \text{(Equation 4-2)}$$

The purpose of this section of the report is to address the impact of the new square cell model results on the existing licensing basis leak rate factors provided in Reference 4-3 for the Model F and Model D5 steam generators. Among the four leakage subfactors identified in Equation 4-2 above, it has been determined that the latest square cell model results affect two of the four subfactors for the Model D5 steam generator only. The subfactors affected are the loss coefficient subfactor (K_{NOP}/K_{DBA}) and the effective crevice length subfactor (l_{NOP}/l_{DBA}). The driving heads (Δp) at both of these conditions are known, as are the temperatures and pressures to define the fluid viscosity (μ). As discussed in References 4-1 and 4-2, the design specification curves for the locked rotor and control rod ejection events apply for the leakage factors for these transients. These transients are of very short duration, for which the H* leakage calculations employ a time integrated leakage approach. The same leakage factors for a postulated locked rotor and control rod ejection event for the Model D5 and F SGs in the H* fleet included in Reference 4-3 continue to apply.

4.1 LOSS COEFFICIENT SUBFACTOR DISCUSSION

4.1.1 Models D5 and F SG Steam Line Break Condition

As discussed in Section 9.1.1 of References 4-1 and 4-2, the current licensing basis leakage factors assume a loss coefficient subfactor of 1.0. The available data for hydraulically expanded tubes in tubesheet simulants (References 4-4 and 4-5), both at room temperature and at elevated temperature, are utilized in References 4-1 through 4-3 to show that no correlation between loss coefficient and contact pressure exists for conditions that simulate the Model D5 SG conditions. However, because the data

exhibit considerable scatter, confidence in this data analysis is low. Engineering judgment could suggest that loss coefficient might be related to the absolute contact pressure between the tubes and the tubesheet. Hence, a requirement was applied to the H* leakage analysis by the regulatory authorities that it is necessary to show that the contact pressure at accident induced conditions exceeds the contact pressure at normal operating conditions ($Pc_{FLB/SLB}$:Pc_{NOP}>1) in order to assume that the loss coefficient subfactor is equal to 1.0. Only the Model D5 is of concern because it cannot be shown that contact pressure at SLB conditions exceeds that at NOP conditions for the Model D5. For the Model F, the SLB contact pressure meets or exceeds the NOP contact pressure in all cases.

The calculated contact pressure results for all models of SG are, to a large degree, dependent on the temperatures at a particular operating condition. The licensing basis for the Model D5 SG includes a SLB condition that differs from the SLB conditions in the licensing basis for the other SG models. The Model D5 SG SLB transient includes a significantly lower temperature; as a result, it cannot be shown that the contact pressures at accident conditions exceed those at normal operating conditions, and the criterion for contact pressure ($Pc_{FLB/SLB}$:Pc_{NOP}>1) is not met. Consequently, it is necessary to utilize a different approach for leakage analysis that does not depend on loss coefficient being independent of contact pressure to show that the accident induced leakage value assumed in the Final Safety Analysis Report (FSAR) is not exceeded.

Concerning the Model D5 steam generators, it has been determined using both thick shell equations and the C^2 model that the contact pressures during steam line break conditions at various elevations between 0 and 21.03 inches at certain radii in the tube bundle do not always exceed the contact pressures during NOP conditions and, therefore, the criterion $Pc_{FLB/SLB}$:Pc_{NOP}>1 is not met. Therefore, it was necessary to determine if the leakage factor for a postulated SLB event remains bounded by the leakage factor for a postulated FLB.

As discussed in detail in Reference 4-6, this involved the development of two alternate approaches for calculating a SLB leakage factor when SLB contact pressures are reduced relative to normal operating condition contact pressures.

The alternate approaches considered were:

1. Parametric assumptions of loss coefficient dependency on contact pressure.
2. Application of parallel plate theory.

Both approaches rely on the existing Model D5 leak rate data to varying degrees. The approach of assuming various proportionality formulations between the loss coefficient and contact pressure and benchmarking them against the existing data is the most direct application. The latter approach utilizes accepted theory to calculate a flow area based on test results and relates that flow area (and consequential leak rate) to the contact pressure conditions for the test specimens to develop leak rates for both SLB and NOP conditions.

Both approaches calculated a SLB leakage factor of less than [ ]^{a,c,e} which remains bounded by the current licensing basis leakage factors for the entire H* fleet with considerable margin. The current licensing basis leakage factors range from 3.11 to 3.27 for a postulated FLB heat-up event.

Concerning the Model F steam generators in the H* fleet, the results of the square cell analysis show that the contact pressure during steam line break conditions at various elevations between 0 and 21.03 inches at all radii in the tube bundle always meets or exceeds the contact pressure during normal operating conditions as shown on Figure 3-24 through Figure 3-29 of this report, thereby meeting the criterion ($Pc_{FLB/SLB}$:Pc_{NOP}>1). Therefore, it is concluded that there is no adverse impact on existing values for the leakage factors defined for the Model F SGs (i.e., the leakage factors calculated for a postulated FLB event still bound the leakage factors calculated for a postulated SLB event). The leakage factors remain the same as in the current licensing basis for the Model F SGs.

4.1.2 Models D5 and F Steam Generator Feedline Break Discussion

For the Model D5 SGs, the contact pressures during a postulated FLB event have been calculated at 9 elevations at 6 different radii using the square cell model. It has been determined that FLB contact pressure always exceeds NOP condition contact pressure at all the tube bundle radii and elevations in the tubesheet as shown in Figure 4-1 through Figure 4-6. Therefore, it remains conservative to apply a ratio of K_{NOP}/K_{DBA} of 1.0 and the current licensing basis leakage factors identified in Reference 4-3 continue to apply.

For the Model F SG, the primary differences in boundary conditions between SLB and FLB are an increase in primary pressure from [ ]^{a,c,e} psia to [ ]^{a,c,e} psia, a hot leg temperature increase from [ ]^{a,c,e} °F to [ ]^{a,c,e} °F, and a cold leg temperature increase from [ ]^{a,c,e} °F to [ ]^{a,c,e} °F. The pressure increase will result in a small increase in tubesheet bending, which will have a minor effect on the through-thickness contact pressure profile. The temperature increase will reduce the elastic moduli of the materials by a small amount, which will also increase the bending slightly, again having a minor impact on through-thickness contact pressure profiles. The temperature increase will also increase the differential thermal growth between the tube and the tubesheet. This is expected to result in overall higher contact pressures for feedline break relative to steam line break (Reference 4-8).

Therefore, for the Model F SG, referring to Figure 3-24 to Figure 3-29 of this report, it is observed that SLB contact pressure meets or exceeds the contact pressure during NOP conditions for all radii of the tube bundle the entire thickness of the tubesheet during a postulated SLB (relative to NOP conditions), therefore, as the contact pressures during a postulated FLB would be expected to increase, it is conservative to apply a ratio of K_{NOP}/K_{DBA} of 1.0.

a,c,e

Figure 4-1 Feedline Break Contact Pressure at 4.437 in. Radius

a,c,e

Figure 4-2 Feedline Break Contact Pressure at 10.431 in. Radius

a,c,e

Figure 4-3 Feedline Break Contact Pressure at 18.139 in. Radius

a,c,e

Figure 4-4 Feedline Break Contact Pressure at 26.703 in. Radius

a,c,e

Figure 4-5 Feedline Break Contact Pressure at 42.974 in. Radius

a,c,e

Figure 4-6 Feedline Break Contact Pressure at 49.825 in. Radius

4.2 EFFECTIVE CREVICE LENGTH SUBFACTOR DISCUSSION

4.2.1 Models D5 and F Steam Line Break Discussion

As discussed in References 4-1 and 4-2, recall that "effective crevice length" is defined as the length of positive contact pressure between the tube and the tubesheet (above H*). For the Model D5 steam generators, the latest square cell model analysis results do not show that positive contact pressure exists throughout the thickness of the tubesheet above the H* distance during both NOP and SLB conditions. Therefore, the effective length ratio subfactor for (l_{NOP}/l_{DBA}) cannot be assumed to be 1.0 during a postulated steam line break event for the Model D5 SGs.

To determine the applicable effective length subfactor based on the C^2 model analysis, the distance of positive contact pressure above the H* distance down from the top of the tubesheet was determined and a new effective length ratio was calculated after the Poisson contraction effect has been considered. Referring to Table 4-1, four of the 6 radii have effective contact pressure ratios greater than 1.0 using the square cell model results.

Despite the length factor increase, no increase in the current licensing basis leakage rate factors reported in Reference 4-3 is necessary because the increase in effective crevice length ratio is counterbalanced by the reduction in viscosity subfactor ratio which occurs as a result of the reduction in primary fluid temperature from hot standby conditions from [ ]^{a,c,e} °F to [ ]^{a,c,e} °F during a postulated SLB event. The viscosity subfactor ratio decreases to [ ]^{a,c,e} (i.e., [ ]^{a,c,e} lbm/ft-sec/[ ]^{a,c,e} lbm/ft-sec (Reference 4-7) from an assumed value of 1.00; 0.49 times the bounding effective crevice length ratio of 1.51 in Table 4-1 is less than 1.

For the Model F SG, it has been determined that the length of positive contact pressure during SLB conditions meets or exceeds the length of positive contact pressure during NOP for all radii in the tube bundle, therefore, the effective crevice length ratio (l_{NOP}/l_{DBA}) is always 1.0 above H*.

Moreover, the leak rate factors defined for the Model D5 and F SGs in References 4-1 and 4-2 are based on a postulated FLB event, not a postulated SLB.

4.2.2 Models D5 and F Feedline Break Discussion

For the Model D5 SG, as discussed in Section 4.1 of this report, it is shown that a positive contact pressure exists throughout the thickness of the tubesheet at all tube bundle radii. Therefore, based on a review of Figure 4-1 through Figure 4-6, the effective crevice length ratio (l_{NOP}/l_{FLB}) remains equal to 1.0 above H* and there is no impact on the current leakage factors identified in Reference 4-3.

For the Model F SG, the primary differences in boundary conditions between SLB and FLB are an increase in primary pressure from [ ]^{a,c,e} psia to [ ]^{a,c,e} psia, a hot leg temperature increase from [ ]^{a,c,e} °F to [ ]^{a,c,e} °F, and a cold leg temperature increase from [ ]^{a,c,e} °F to [ ]^{a,c,e} °F. The pressure increase will result in a small increase in tubesheet bending, which will have a minor effect on the through-thickness contact pressure profile. The temperature increase will reduce the elastic moduli of the materials by a small amount, which will also increase the bending slightly, again having a minor impact on through-thickness contact pressure profiles. The temperature increase will also increase the

differential thermal growth between the tube and the tubesheet. This is expected to result in overall higher contact pressures for feedline break relative to steam line break (Reference 4-8).

For the Model F SG, it has been determined that the length of positive contact pressure during SLB conditions meets or exceeds the length of positive contact pressure during NOP for all radii of the tube bundle, therefore, as the contact pressures during a postulated FLB would be expected to be higher, the effective crevice length ratio (l_{NOP}/l_{DBA}) is always equal to 1.0.

4.3 C^2 MODEL LEAKAGE INTEGRITY SUMMARY

Based on Sections 4.1 and 4.2 above, it is concluded that the current licensing basis leakage factors identified in Reference 4-3 continue to apply when considering the C^2 model results.

Table 4-1 Model D5 Crevice Length Subfactors Based on C^2 Model Contact Pressure Profiles

	Tube Bundle Radius (Inches)						
Model D5	**4.437**	**10.431**	**18.139**	**26.703**	**42.974**	**49.825**	
Length (NOP) inches[1]	[						a,c,e
Length (SLB) inches[1]	[						a,c,e
H* Value	14.01	14.01	14.01	14.01	14.01	14.01	
Length Above H* (NOP)[2]	[						a,c,e
Length Above H* (SLB)[2]	[						a,c,e
Revised (l_{NOP}/l_{SLB}) Subfactor	[						a,c,e

Notes:
1. Distance from the bottom of the tubesheet with positive contact pressure.
2. Distance above 95/95 H* of 14.01 inches with positive contact pressure.
3. Distance includes an allowance of 0.3 inch for the location of the bottom of the expansion transition from the top of the tubesheet.

4.4 REFERENCES

4-1. WCAP-17071-P, Rev. 2, "H*: Alternate Repair Criteria for the Tubesheet Expansion Region in Steam Generators with Hydraulically Expanded Tubes (Model F)," September 2010.

4-2. WCAP-17072-P, "H*: Alternate Repair Criteria for the Tubesheet Expansion Region in Steam Generators with Hydraulically Expanded Tubes (Model D5)," May 2009.

4-3. LTR-SGMP-09-100 P-Attachment, Rev. 1, "Responses to NRC Request for Additional Information on H*; Model F and Model D5 Steam Generators," September 2010.

4-4. CN-SGDA-03-119, Rev. 1, "Calculation of Loss Coefficient for Model D5 Steam Generators," Westinghouse Electric Company LLC, June 2004.

4-5. STD-MCE-03-49, "Determination of Model D5 Tube-to-Tubesheet Leakage Resistance for H-Star Program for CBE/CDE/DDP/TCX," November 4, 2003.

4-6. LTR-SGMP-10-95 P-Attachment, Rev. 1, "H*: Alternate Leakage Calculation Methods for H* for Situations When Contact Pressure at Normal Operating Conditions Exceeds Contact Pressure at Accident Conditions," September 2010.

4-7. Dynamic Viscosity Data from Isothermal Properties of Water, National Institute of Standards and Technology, Online Data Base, webbook.nist.gov.

4-8. LTR-SGMP-10-135, "Assessment of Feedwater Line Break Conditions on Contact Pressures for Model F for H*," October 26, 2010.

5 REPORT SUMMARY AND CONCLUSIONS

The purpose of this report is to provide final resolution of the NRC technical issue regarding tubesheet bore eccentricity on the H* criterion. As a result, the NRC staff asked 14 questions related to this issue. As stated in Section 1of this report, the content of this report primarily focuses on resolving NRC Request for Additional Information (RAI) Numbers 5 and 12. A roadmap was provided in Section 1 to previous documents issued by Westinghouse in response to the remainder of the 14 RAIs.

There are two principal requirements for H*:

1. Assure that tube(s) do not pull out of the tubesheet under the most limiting loadings during normal or accident conditions.

2. Assure that primary-to-secondary leakage through the tube-to-tubesheet crevice is no greater than that assumed in the final safety analysis report (FSAR) for the most limiting accident.

Concerning Item 1, the Westinghouse action plan to resolve the NRC staff tube pull out concerns relating to tube bore eccentricity involved the development of a more accurate analysis model for calculating tube joint contact pressure. As discussed in Section 3 of this report, the square cell (C^2) model analysis is an independent method of modeling the contact pressure distribution between the tube and the tubesheet throughout the tubesheet thickness.

Consistent application of a single structural model showed that the limiting condition for the Model D5 plants is the SLB condition, rather than the NOP conditions as documented in the current licensing basis (Reference 5-3). For the Model D5 SG for the limiting plant, the value of H* inspection depth required to meet the structural integrity goals of the plant decreased by 2.94 inches; whereas, the value for the limiting plant for the Model F SGs increased by 2.19 inches. The differences between the two models are the results of different end cap loads, tubesheet displacements and contact pressure distributions. A direct comparison between the licensing basis probabilistic H* values and the square cell analysis probabilistic H* values for the Model F and Model D5 steam generators is shown in Table 5-1. The H* values provided in Table 5-1 provide tube pull out capability that meet or exceed the structural integrity acceptance criteria identified in Section 4.1 of References 5-2 and 5-3.

The impact of the new square cell model results on the existing licensing basis leak rate factors provided in Reference 5-5 for the Model F and Model D5 steam generators was evaluated. Of the four leakage subfactors identified in References 5-2 and 5-3, it was determined that the square cell model results affect two of the four subfactors for the Model D5 steam generator during the postulated SLB event. The subfactors affected are the loss coefficient subfactor (K_{NOP}/K_{SLB}) and the effective crevice length subfactor (l_{NOP}/l_{SLB}).

Relative to the loss coefficient subfactor for leakage, as discussed in Section 4 of this report, the licensing basis for the Model D5 SG includes a SLB condition that differs from the SLB conditions in the licensing basis for the Model F SG. The Model D5 SG SLB transient includes a significantly lower temperature; as a result, it cannot be shown that the contact pressures at accident conditions exceed those at normal operating conditions, and the NRC criterion for contact pressure ($Pc_{SLB}:Pc_{NOP}>1$) is not met, implying that a loss coefficient subfactor of 1.0 cannot be justified. This was determined to be the case using both the

thick shell equation model and the C^2 model to calculate tube joint contact pressures. Consequently, it was necessary to utilize a different approach for leakage analysis that does not depend on loss coefficient being independent of contact pressure to show that the accident induced leakage value assumed in the FSAR is not exceeded.

Two alternate approaches were considered:

1. Parametric assumptions of loss coefficient dependency on contact pressure.
2. Application of parallel plate theory.

Both approaches calculated a SLB leakage factor of less than [ ]^{a,c,e} (Reference 5-1) which remains bounded by the current licensing basis factors for the H* fleet for the Model D5 SGs with considerable margin.

Relative to the effective crevice length subfactor, it has been determined that a subfactor > 1.0 exists during a postulated SLB for a Model D5 SG at certain radii. This is the case because, according to the square cell model results, positive contact pressure does not exist for the same distance above H* during normal operating and postulated SLB conditions. The length of positive contact pressure decreases during a postulated SLB event which results in a bounding leakage subfactor of [ ]^{a,c,e} (see Section 4.2.1). However, this larger subfactor is counterbalanced by the reduction in dynamic viscosity that occurs during a postulated SLB due to the greater than 250 °F reduction in primary fluid temperature that occurs during the transient.

For the Model D5 SGs, the leakage factors range from 3.11 to 3.27 (References 5-5 and 5-8) for a postulated FLB heat up event. It has been confirmed that it remains conservative to apply a value 1.0 for both the leakage subfactor for loss coefficient and effective crevice length during a postulated FLB for the Model D5 SG. The results from application of the square cell model analysis verify that contact pressure increases during a postulated FLB relative to normal operating plant conditions at all tube bundle radii and elevations. It also has been verified that positive contact pressure exists at all radii and tubesheet elevations. Therefore, the leakage rate factors identified in the current licensing basis (Reference 4-3) continue to apply for the Model D5 SGs.

Finally, using either the thick shell equation or the C^2 model approach, results show that the contact pressures during SLB conditions at elevations above H* at all radii in the tube bundle always meets or exceeds the contact pressures during normal operating conditions for the Model F SGs. Based on a qualitative assessment of the factors that impact contact pressures, it is concluded that contact pressure increases during a postulated FLB relative to a postulated SLB for the Model F SG. Therefore, no alternate method for leakage analysis is required and the current licensing basis leakage factor values identified in the current licensing basis (References 5-5 and 5-8) continue to apply for the Model F SGs.

Concerning all other design basis accidents that model accident condition leakage, as discussed in References 5-2 and 5-3, the design specification curves for the locked rotor and control rod ejection events apply for the leakage factors for these transients. These transients are of very short duration and the H* leakage calculations employ a time integrated leakage approach. The same leakage factors for a postulated locked rotor and control rod ejection event for the Model D5 and F SGs in the H* fleet included in the current licensing basis (References 5-5 and 5-8) continue to apply.

Based on the above, with the use the leakage factors included in the current licensing basis (References 5-5 and 5-8), it is concluded that primary-to-secondary leakage through the tube-to-tubesheet crevice is bounded by the values assumed in the final safety analysis report (FSAR) for the most limiting accident.

Satisfactory resolution of the NRC technical issue regarding tubesheet bore eccentricity is complete. Together with documents provided under separate cover, (e.g., Reference 5-6) this document completes the response to the RAI provided in Reference 5-7. Application of the C^2 model has provided independent confirmation that the structural criteria are met. Probabilistic H* values were re-calculated based on application of the C^2 model. The differences between the H* results based on the C^2 model and those from the prior application of the thick shell model are explained. The leakage factors contained in the current licensing basis for the Model D5 and Model F SGs are shown to be conservative and acceptable for implementation of H*.

Table 5-1 Results of Probabilistic Comparison Study for the Limiting Plants in the H* Fleet

			Thick Shell Calculations			Square Cell Calculations			
			(Reference 5-4)		Implemented H*[1]	Whole Bundle		Whole Plant	
SG Model/ Limiting Plant	Limiting Operating Condition	Current Licensing Basis	95/50 Whole Bundle	95/95 Whole Plant	Plant Tech. Spec.	95/50	95/95	95/50	95/95
			in	in	in	in	in	in	in
Model F/ Millstone Unit 3	NOP	WCAP-17071-P	11.20	13.02	13.10	N/A	[ ]^{a,c,e}	15.13	15.21
Model D5/ Byron & Braidwood Unit 2	SLB	WCAP-17072-P	13.80	16.95	16.95	14.00	14.01	N/A	N/A

Note:
1. Values taken from utilities' 2009 license amendment requests.

5.1 REFERENCES

5-1. LTR-SGMP-10-95 P-Attachment, Rev. 1, "H*: Alternate Leakage Calculation Methods for H* for Situations When Contact Pressure at Normal Operating Conditions Exceeds Contact Pressure at Accident Conditions," September 2010.

5-2. WCAP-17071-P, Rev. 2, "H*: Alternate Repair Criteria for the Tubesheet Expansion Region in Steam Generators with Hydraulically expanded Tubes (Model F)," September 2010.

5-3. WCAP-17072-P, "H*: Alternate Repair Criteria for the Tubesheet Expansion Region in Steam Generators with Hydraulically Expanded Tubes (Model D5)," May 2009.

5-4. LTR-SGMP-09-104 P-Attachment, Rev. 1, "White Paper on Probabilistic Assessment of H*," August 13, 2009.

5-5. LTR-SGMP-09-100 P-Attachment, Rev. 1, "Responses to NRC Request for Additional Information on H*; Model F and Model D5 Steam Generators," September 2010.

5-6. LTR-SGMP-10-33 P-Attachment, "H*: Response to NRC Questions Regarding Tubesheet Bore Eccentricity," September 2010.

5-7. USNRC Letter, "Vogtle Electric Generating Plant, Units 1 and 2 – Transmittal of Unresolved Issues Regarding Permanent Alternate Repair Criteria for Steam Generators (TAC Nos. ME 1339 and ME 1340)," November 23, 2009.

5-8. USNRC Letter, "Catawba Nuclear Station, Unit 2, Issuance of Amendment Regarding the Steam Generator Program (TAC No. ME4108)," September 27, 2010.